Inorganic Chemistry
Cite This: Inorg. Chem. XXXX, XXX, XXX−XXX
Article
pubs.acs.org/IC

Electrochemical, Spectroelectrochemical, and Structural Studies of Mono- and Diphosphorylated Zinc Porphyrins and Their Self-Assemblies

Yuanyuan Fang,[†] Xiaoqin Jiang,[†] Karl M. Kadish,[*,†] Sergey E. Nefedov,[‡] Gayane A. Kirakosyan,[‡,§] Yulia Y. Enakieva,[§,∥] Yulia G. Gorbunova,[‡,§] Aslan Y. Tsivadze,[‡,§] Christine Stern,[∥] Alla Bessmertnykh-Lemeune,[*,∥] and Roger Guilard[∥]

[†]Department of Chemistry, University of Houston, Houston, Texas 77204-5003, United States
[‡]Kurnakov Institute of General and Inorganic Chemistry, Russian Academy of Sciences, Leninsky Pr. 31, Moscow, 119991, Russia
[§]Frumkin Institute of Physical Chemistry and Electrochemistry, Russian Academy of Sciences, Leninsky Pr. 31, build. 4, Moscow, 119071, Russia
[∥]Institut de Chimie Moléculaire de l'Université de Bourgogne, Université Bourgogne Franche-Comté, UMR CNRS 6302, 9 Avenue Alain Savary, BP 47870, Dijon 21078 CEDEX, France

Supporting Information

ABSTRACT: Three series of porphyrins containing a Zn(II) central metal ion and zero, one, or two phosphoryl groups at the *meso*-positions of the macrocycle were characterized as to their electrochemical, spectroscopic, and structural properties in nonaqueous media. The investigated compounds are represented as 5,15-bis(4′-R-phenyl)porphyrinatozinc, 10-(diethoxyphosphoryl)-5,15-bis(4′-R-phenyl)porphyrinatozinc, and 5,15-bis(diethoxyphosphoryl)-10,20-bis(4′-R-phenyl)porphyrinatozinc, where R = OMe, Me, H, or CN. Linear-free energy relationships are observed between the measured redox potentials at room temperature and the electronic nature of the substituents at the 5 and 15 *meso*-phenyl groups of the macrocycle. The mono- and bis-phosphoryl derivatives with two *p*-cyanophenyl substituents provide electrochemical evidence for aggregation at low temperature, a greater degree of aggregation being observed in the case of 5,15-bis(diethoxyphosphoryl)-10,20-bis(4′-cyanophenyl)porphyrinatozinc(II). This compound was characterized in further detail by variable-temperature ^{1}H and $^{31}P\{^{1}H\}$ NMR spectroscopy in solution combined with single crystal X-ray analysis in the solid state. The data obtained from these measurements indicate that this porphyrin has a dimeric structure in $CDCl_3$ at 223−323 K but forms a 2D polymeric network when it is crystallized from a $CHCl_3$/MeOH mixture.

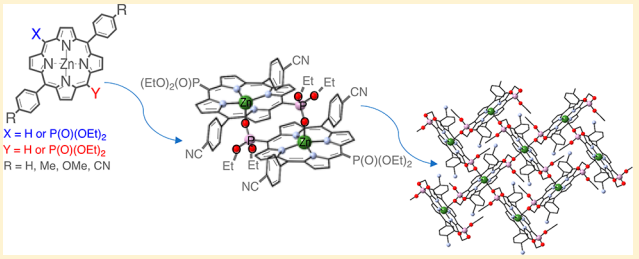

INTRODUCTION

Porphyrins and related tetrapyrrolic macrocycles are widely used by living systems for the optimal organization of important processes such as oxygen transport, catalytic reactions, light-harvesting, photoinduced charge separation, and electron transport.[1−4] Synthetic porphyrins have unparalleled significance for understanding these naturally occurring processes[5−8] and are regarded as a way of dealing more efficiently with major societal challenges.[9−14] The physicochemical features of these pigments have continued to attract attention from scientists in the fields of physics, biology, medicine, material science, and burgeoning new areas such as molecular recognition and nanotechnology.

It has been well documented in the literature that the physicochemical properties of porphyrins can be dramatically tuned by introducing substituents with different electronic and steric effects at the periphery of the macrocycle.[14] One key strategy to adapt the structural properties of porphyrin molecules to a target task is to vary the substitution pattern of aryl groups at the *meso*-positions of the porphyrin macrocycle. The synthesis of porphyrins bearing functional groups directly attached to the macrocycle has also been widely investigated, and powerful synthetic strategies based on transition-metal-catalyzed carbon−carbon and carbon−heteroatom (N, O, S, Se, B) bond forming reactions have been developed.[15−24] However, the low air and photostability of many porphyrins bearing electron-donating functional groups at the macrocycle periphery is a serious drawback for their practical application. In this context, electron-deficient withdrawing phosphorus(V)-substituted porphyrins are of particular interest, since these compounds have been shown to be highly stable.

Received: January 29, 2019

DOI: 10.1021/acs.inorgchem.9b00268
Inorg. Chem. XXXX, XXX, XXX−XXX

The first examples of *meso*-phosphorylporphyrins prepared from *meso*-haloporphyrins under palladium- and copper-catalyzed conditions were reported independently by the groups of Arnold and Matano.[25−27] Later, palladium catalysts were employed to facilitate the reaction of readily accessible *meso*- and *β*-bromoporphyrins with dialkyl phosphites, giving a concise and versatile method for preparing porphyrinylphosphonic acid derivatives in reasonably good yield.[28−30] In particular, many new A_2B-, A_2BC-, and *trans*-A_2B_2-type porphyrins (B = diethoxyphosphoryl) were prepared taking advantage of the relatively simple separation of the target molecules from crude mixtures of the polar porphyrin derivatives.[31]

These photo- and air-stable porphyrin pigments with phosphoryl groups show promise for high-value-added applications in the areas of energy production, optoelectronics, fine chemicals synthesis, and health care.[26,27,32−43] For instance, porphyrinylphosphonic acids and their monoalkyl esters have led to the preparation of water-soluble porphyrins which have been extensively investigated for use in biomedicine (e.g., molecular imaging, photodynamic therapy, and oxygen detection).[34,44] Several investigations of hybrid organic−inorganic materials have demonstrated that transition metal complexes containing phosphonate anchoring groups can be easily heterogenized by grafting onto metal oxides or through the incorporation in coordination polymer networks.[45−52] These are attractive synthetic routes to prepare detectors, sensitizers, and catalysts based on porphyrin derivatives.

In addition, phosphorylporphyrins are important molecular building blocks for the elaboration of supramolecular porphyrin assemblies which mimic natural photosynthesis processes.[27,29,38,53,54] Indeed, the phosphoryl group is an oxygen donor which can axially ligate the central metal ion of another porphyrin molecule or bind to external metal ions, giving coordination-assembled porphyrin systems. These molecular algorithms can then be used in crystal engineering or in solution chemistry to prepare elaborate coordination frameworks.[28,55]

An understanding of the electrochemical properties of phosphorylated porphyrins should provide a solid basis for the design and optimization of these compounds' properties when employed in electron-transfer processes, catalytic reactions, and crystal engineering as molecules, supramolecular architectures, or hybrid functional materials. The addition of one or more phosphoryl groups to a porphyrin macrocycle can significantly modify chemical and physical properties of the compound, with the type and magnitude of the effect being dependent in large part on the position of the substituents. In this regard, three series of phosphorylated porphyrins have to date been examined as to their electrochemical properties. These are (i) *meso*-4′-(diethoxyphosphoryl)phenyl substituted derivatives,[53] (ii) *β*-pyrrole substituted porphyrins,[54] and (iii) *meso*-phosphorylporphyrins.[53,56]

In the current paper, we describe electrochemical and spectroscopic properties for three series of Zn(II) porphyrins containing phosphoryl groups on the *meso*-positions of the macrocycle. Structures of the investigated porphyrins are shown in Chart 1 and are represented as 5,15-bis(4′-R-phenyl)porphyrinatozinc (**1a−d**), 10-(diethoxyphosphoryl)-5,15-bis(4′-R-phenyl)porphyrinatozinc (**2a−d**), and 5,15-bis-(diethoxyphosphoryl)-10,20-bis(4′-R-phenyl)porphyrinatozinc (**3a−d**).

Chart 1. Structure of the Investigated Porphyrins

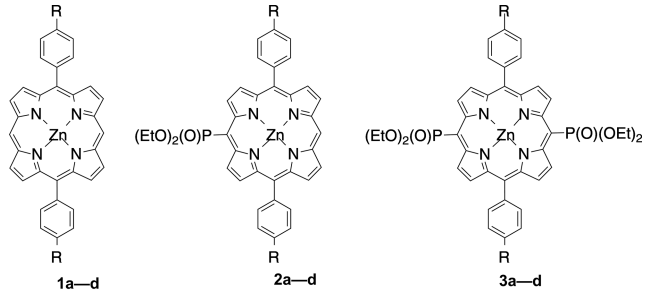

a = R = OMe; **b** R = Me; **c** R = H; **d** R = CN

The phosphoryl groups on the porphyrins of Chart 1 are electron-withdrawing, and these derivatives have been earlier demonstrated to undergo more facile reductions at the porphyrin macrocycle than the related tetraphenylporphyrins with the same central metal ions.[53] More importantly, a coordination self-assembly was previously observed for structurally related *β*- and *meso*-phosphorylated Zn(II) porphyrins,[27,54] and these self-assemblies were sometimes electrochemically detected at low temperature by a splitting of the first oxidation process,[27,54] suggesting the presence of equivalent and interacting redox centers in the molecule.

Another example for the electrochemical detection of phosphorylporphyrin self-aggregation is given by the methoxyphenyl-containing compound **3a** in Chart 1 where the current−voltage curves for reduction by cyclic voltammetry in CH_2Cl_2 suggested the presence of monomers at room temperature but aggregates when the measurements on a 10^{-3} M solution were carried out at −75 °C.[53] UV−visible data for the same compound in $CDCl_3$ indicated the presence of a concentration dependent equilibrium, where monomers were present at 10^{-6} M and aggregates at 10^{-4} M.[53] No explanation was given in the paper for this apparently contradictory data for millimolar solutions of the porphyrin at room temperature, but the fact that the monomeric species were easier to electrochemically reduce than the aggregate by 150 mV in CH_2Cl_2 would favor conversion of any higher porphyrin aggregates in solution to the more easily reducible monomer at the electrode surface under the application of an applied potential.

This is further investigated in the current study for the mono- and bis-phosphoryl series of compounds in Chart 1 where we wished to also examine how the electrochemically detected self-aggregation on reduction would be effected by increasing the number of electron-withdrawing *meso*-P(O)-$(OEt)_2$ groups on the porphyrin from one to two while also increasing the electron-withdrawing properties of the *para*-substituent on the two *meso*-phenyl rings of the compounds, from OMe on one extreme to CN on the other.

As it will be shown, a well-defined splitting of the first reduction potential is observed at low temperature for the CN-phenyl containing porphyrins **2d** and **3d**, again indicating a coordination self-assembly of these complexes under the electrochemical solution conditions. The largest degree of self-assembly under the electrochemical conditions was observed for compound **3d**, and this porphyrin was then further investigated by variable-temperature ^1H and $^{31}P\{^1H\}$ NMR spectroscopies in solution and single crystal X-ray diffraction in the solid state. When crystals of the 2D coordination polymer $(\mathbf{3d})_n$ were dissolved in chloroform, an

DOI: 10.1021/acs.inorgchem.9b00268
Inorg. Chem. XXXX, XXX, XXX−XXX

interesting structural modification was observed, leading to the formation of dimer $(\mathbf{3d})_2$. This is the first example of a phosphorylporphyrin exhibiting a dimeric structure in chloroform at room temperature and also displaying different supramolecular organization in crystals and in solution.

EXPERIMENTAL SECTION

General Considerations. Unless otherwise noted, all chemicals were obtained commercially from Acros or Aldrich and used without further purification. Tetra-*n*-butylammonium perchlorate (TBAP) was purchased from Sigma-Aldrich Co. ***Caution!*** *Perchlorate salts are potentially explosive and should be handled with care.*

[5,15-Bis(4′-methoxyphenyl)porphyrinato(2-)]zinc (**1a**),[57] [5,15-bis(4′-methylphenyl)porphyrinato(2-)]zinc (**1b**),[58] 5,15-bis(4′-phenyl)porphyrinato(2-)]zinc (**1c**),[58] [5,15-bis(4′-cyanophenyl)porphyrinato(2-)]zinc (**1d**),[42] [10-(diethoxyphosphoryl)-5,15-bis(4′-methoxyphenyl)porphyrinato(2-)]zinc (**2a**),[58] [10-(diethoxyphosphoryl)-5,15-bis(4′-tolyl)porphyrinato(2-)]zinc (**2b**),[58] [10-(diethoxyphosphoryl)-5,15-diphenylporphyrinato(2-)]zinc (**2c**),[58] [10-(diethoxyphosphoryl)-5,15-bis(4′-cyanophenyl)porphyrinato(2-)]zinc (**2d**),[58] [5,15-bis(diethoxyphosphoryl)-10,20-bis(4′-tolyl)porphyrinato(2-)]zinc (**3b**),[53] [5,15-bis(diethoxyphosphoryl)-10,20-bis(phenyl)porphyrinato(2-)]zinc (**3c**),[28,53] [10-bromo-5,15-bis(4′-methoxyphenyl)porphyrinato(2-)]zinc (**4a**),[58] [10-bromo-5,15-bis(4′-tolyl)porphyrinato(2-)]zinc (**4b**),[58] [10-bromo-5,15-bis(phenyl)porphyrinato(2-)]zinc (**4c**),[28,53] [10-bromo-5,15-bis(4′-cyanophenyl)porphyrinato(2-)]zinc (**4d**),[58] [5,10-dibromo-10,20-bis(4′-tolyl)porphyrinato(2-)]zinc (**5b**),[53] and 5,10-dibromo-10,20-bis(phenyl)porphyrinato(2-)]zinc (**5c**)[53] were prepared according to published procedures.

Reactions were performed in air unless otherwise noted. Column chromatography purification was carried out on silica gel (Silica 60, 63−200 μm, Aldrich). Analytical thin-layer chromatography (TLC) was carried out using Merck silica gel 60 F-254 plates (precoated sheets, 0.2 mm thick, with fluorescence indicator F254). All solvents were dried by standard procedures (dichloromethane: distillation from CaH_2; absolute EtOH: distillation over Mg; benzonitrile: distillation over P_2O_5; toluene: distillation over sodium).

^1H and $^{31}P\{^1H\}$ NMR spectra were acquired on Bruker Avance III 600 MHz, 500 MHz and Avance II 300 MHz and Nanobay 300 MHz spectrometers and referenced to the solvent residual protons ($CDCl_3$, 7.24 ppm) and concentrated H_3PO_4, respectively.

Diffusion ordered NMR ^1H DOSY measurements were carried out on a Bruker Avance III 600 MHz spectrometer equipped with a standard 10 A gradient amplifier and a BBO probe head with a PFG *Z*-axis coil having a gradient strength of 5.57 G/cm A. Spectra were recorded at 323 K, using the standard Bruker Topspin 3.2 dstegp3s pulse sequence employing double stimulated echo and longitudinal eddy delay with 3 spoil gradients. Smoothed chirp pulses with 2 ms duration were used. The strength of gradient pulses was varied linearly from 5% to 95% of the maximum current (10 A) in 16 steps. For each increment, 8 transients (+ four dummy scans) were acquired into 128k data points using a spectral width of 15 000 Hz. All increments were corrected for phase and baseline distortions before mono-exponential fitting into 256k points in the diffusion dimension using the T1/T2 analysis module of Topspin 3.2.

UV−visible spectra of the compounds were obtained on a Varian Cary 50 spectrophotometer by using a rectangular quartz cell (Hellma, 100-QS, 45 × 12.5 × 12.5 mm, path length: 10 mm, chamber volume: 3.5 mL).

MALDI-TOF mass spectra were obtained on a Bruker Ultraflex II LRF 2000 mass spectrometer in positive ion mode with a dithranol matrix. Accurate mass measurements (HRMS) were made on a THERMO LTQ Orbitrap XL equipped with an electrospray ionization (ESI) source in positive mode unless otherwise stated. Solutions in $CHCl_3$/methanol (1:1) were used for the analysis.

IR spectra were registered on Nicolet Nexus and Bruker Vector 22 FT-IR spectrophotometers. A universal micro-ATR sampling accessory (Pike) was used in order to obtain IR spectra of solid samples.

All of the spectrometers except for the Nexus (Nicolet) spectrophotometer and the Bruker Avance III 600 MHz and Avance II 300 MHz spectrometers (Shared Facility Centers at the Institute of Physical Chemistry and Electrochemistry RAS and Institute of General and Inorganic Chemistry RAS, respectively) were available at the "Pôle Chimie Moléculaire", the technological platform for chemical analysis and molecular synthesis (http://www.wpcm.fr) which relies on the Institute of the Molecular Chemistry of University of Burgundy and WelienceTM, a Burgundy University private subsidiary.

Cyclic voltammetry was carried out at 298 K using an EG&G Princeton Applied Research (PAR) 173 potentiostat/galvanostat. A homemade three-electrode cell was used for cyclic voltammetric measurements and consisted of a glassy carbon working electrode, a platinum counter electrode, and a homemade saturated calomel reference electrode (SCE). The SCE was separated from the bulk of the solution by a fritted glass bridge of low porosity, which contained the solvent/supporting electrolyte mixture.

Thin-layer UV−vis spectroelectrochemical experiments were performed using a home-built thin-layer cell, which has a transparent platinum net working electrode. Potentials were applied and monitored with an EG&G PAR Model 173 potentiostat. High purity N_2 from Trigas was used to deoxygenate the solution and kept over the solution during each electrochemical and spectroelectrochemical experiment.

Crystals suitable for single crystals X-ray analysis were grown by a slow diffusion of heptane in an open glass tube of **3d** in a $CHCl_3$/MeOH solvent mixture (97:3 v/v, $c = 10^{-3}$ M). Details on the SCXRD experiment and refinement are given in the Supporting Information. Crystallographic data can be obtained free of charge from The Cambridge Crystallographic Data Centre via www.ccdc.cam.ac.uk/data_request/cif (CCDC 1890813).

Powder XRD experiment was carried out on a Bruker D8 Advance Diffractometer with a goniometer radius of 217.5 mm, Göbel Mirror parallel-beam optics, 2° Sollers slits, and 0.2 mm receiving slit. PXRD patterns from 3° to 45° 2θ were recorded at room temperature using Cu Kα radiation (1.5418 Å) under the following measurement conditions: tube voltage of 40 kV, a tube current of 40 mA, step scan mode with a step size of 0.02° 2θ, and a counting time of 2.5 s/step. The sample of porphyrin **3d** was analyzed without being crushed. The crystal X-ray diffraction analysis was performed at the Shared Facility Center of the Kurnakov Institute of General and Inorganic Chemistry of RAS.

Synthesis of Porphyrins 5a and 5d. *General Procedure for Bromination of [5,15-Diarylporphyrinato(2-)]zinc.* [5,15-Diarylporphyrinato(2-)]zinc (1 equiv) and pyridine (10 equiv) were dissolved in chloroform (4 mM), and the resulting mixture was stirred for 15 min at room temperature. After cooling the reaction mixture to the relevant temperature, NBS (2.2 equiv) was added in one portion. The reaction mixture was stirred for 20 min, then quenched with acetone (3 mL) and concentrated under reduced pressure. The resulting crude solid was purified on a short silica gel column using a $CHCl_3$/methanol mixture as an eluent to afford the dibromides **5a** and **5d**. Spectral data of compounds **5a,d** are presented in the SI (Figures S9−S14).

*[5,15-Dibromo-10,20-bis(4′-methoxyphenyl)porphyrinato(2−)]-zinc (**5a**).*[59] The dibromide was prepared from [5,15-bis(4′-methoxyphenyl)porphyrinato(2-)]zinc (**1a**) (74 mg, 0.13 mmol). The reaction was performed at −40 °C. The solid residue was chromatographed using a $CHCl_3/CH_3OH$ (97:3, v/v) mixture as an eluent to give porphyrin **5a** as a purple crystalline powder in 58% yield (55 mg). ^1H NMR (300 MHz, $CDCl_3/CD_3OD$, 2:1 v/v, 25 °C): δ = 9.40 (d, $^3J_{H,H}$ = 4.7 Hz, 4H, Hβ), 8.64 (d, $^3J_{H,H}$ = 4.7 Hz, 4H, Hβ), 7.82 (d, $^3J_{H,H}$ = 8.5 Hz, 4H, *o*-Ph), 7.05 (d, $^3J_{H,H}$ = 8.5 Hz, 4H, *m*-Ph) ppm. MS (MALDI-TOF): *m*/*z* calcd. for $C_{34}H_{22}Br_2N_4O_2Zn$ $[M]^+$ 739.9; found 739.7. UV−vis ($CHCl_3$): λ_{max} [log (ε/M^{-1} cm^{-1})] = 430 (5.55), 566 (4.33), 608 (4.17) nm.

DOI: 10.1021/acs.inorgchem.9b00268
Inorg. Chem. XXXX, XXX, XXX−XXX

*[5,15-Dibromo-10,20-bis(4′-cyanophenyl)porphyrinato(2−)]zinc (**5d**).*[58] The dibromide was prepared from 5,15-bis(4′-cyanophenyl)-porphyrinato(2-)]zinc (**1d**) (20 mg, 0.035 mmol). The reaction was performed at −20 °C. The crude product was purified by column chromatography using a $CHCl_3$/MeOH (99:1, v/v) mixture as an eluent to give porphyrin **5d** as a purple crystalline powder in 98% yield (25 mg). ^{1}H NMR (300 MHz, $CDCl_3$, 25 °C): δ = 9.72 (d, $^3J_{H,H}$ = 4.7 Hz, 4H, Hβ), 8.77 (d, $^3J_{H,H}$ = 4.7 Hz, 4H, Hβ), 8.27 and 8.07 (AB system, J_{AB} = 8.1 Hz, 8 H, *m*-Ph and *o*-Ph, respectively) ppm. MS (MALDI-TOF): *m*/*z* calcd. for $C_{34}H_{16}Br_2N_6Zn$ [M + H]$^+$ 730.9; found 732.2. UV−vis ($CHCl_3$): λ_{max} [log (ε/M^{-1} cm^{-1})] = 431 (5.47), 565 (4.17), 606 (3.82) nm.

*[5,15-Bis(diethoxyphosphoryl)-10,20-bis(4′-methoxyphenyl)porphyrinato(2−)]zinc (**3a**).* A two-neck round-bottom flask equipped with a condenser, a magnetic stirrer bar, and a gas outlet was charged with dibromoporphyrin **5a** (46 mg, 0.062 mmol) and $Pd(PPh_3)_4$ (0.018 mg, 0.015 mmol). The reaction vessel was evacuated and purged with nitrogen three times. Subsequently, a mixture of anhydrous toluene and ethanol (1:1 v/v, 3 mL), diethyl H-phosphonate (3.1 mmol, 0.396 mL), and NEt_3 (0.928 mmol, 0.130 mL) were added by syringes. The reaction mixture was stirred at reflux for 1 day when monitored by MALDI-TOF and ^{1}H NMR. After complete conversion of dibromide **5a** and [5-bromo-15-diethoxyphosphoryl-10,20-bis(4′-methoxyphenyl)porphyrinato(2−)]zinc, the reaction mixture was cooled to room temperature and concentrated under reduced pressure. The solid residue was taken up in chloroform and subjected to column chromatography on silica gel using a $CHCl_3$/CH_3OH mixture (98:2, v/v) as an eluent. Three fractions containing porphyrins were obtained. These solids were characterized as 5,15-bis(4′-methoxyphenyl)porphyrin,[60] compound **2a**[58] (31% yield), and a mixture of porphyrin **3a** with triphenylphosphine oxide in a 1:1 molar ratio (37.5 mg). A further purification of porphyrin **3a** by column chromatography on silica gel using different eluents was unsuccessful. Therefore, to obtain a pure solid, the product was transformed into the corresponding free base porphyrin, purified, and reacted with a zinc salt according to the following procedures.

Trifluoroacetic acid (0.25 mL) was added to the crude solution (37.5 mg) in $CHCl_3$ (37 mL), and the resulting mixture was stirred at room temperature for 3 h. After washing with aqueous $NaHCO_3$ (2 × 15 mL) and water (1 × 15 mL), the reaction mixture was dried over $MgSO_4$ and concentrated under reduced pressure. The solid residue was taken up in CH_2Cl_2 and chromatographed on silica gel using a CH_2Cl_2/CH_3OH mixture (99.5:0.5, v/v) as an eluent to afford 5,15-bis(diethoxyphosphoryl)-10,20-bis(4′-methoxyphenyl)porphyrin (23 mg, 88%). Then, 5,15-bis(diethoxyphosphoryl)-10,20-bis(4′-methoxyphenyl)porphyrin (23 mg, 0.029 mmol) and zinc acetate dihydrate (31.8 mg, 0.145 mmol) in a $CHCl_3$ (9 mL)/CH_3OH (0.5 mL) mixture was stirred at room temperature for 2 h. Then, the reaction mixture was washed with water (3 × 10 mL) to remove an excess of $Zn(OAc)_2{\cdot}2H_2O$. The organic layer was dried over $MgSO_4$ and concentrated under reduced pressure. The resulting crude solid was purified by column chromatography on silica gel using a $CHCl_3$/CH_3OH mixture (98:2, v/v) as an eluent to afford **3a** (23.8 mg, 96%). The yield of porphyrin **3a** calculated on the dibromide **5a** is 45%.

5,15-Bis(diethoxyphosphoryl)-10,20-bis(4′-methoxyphenyl)-porphyrin. ^{1}H NMR (300 MHz, $CDCl_3$/CD_3OD, 2:1 v/v, 25 °C): δ 9.98 (d, $^3J_{H,H}$ = 5.0 Hz, 4H, Hβ), 8.70 (d, $^3J_{H,H}$ = 5.1 Hz, 4H, Hβ), 7.87 (d, $^3J_{H,H}$ = 8.6 Hz, 4H, *o*-Ph), 7.12 (d, $^3J_{H,H}$ = 8.6 Hz, 4H, *m*-Ph), 4.35−4.24 (m, 4H, CH_2O), 4.10−3.97 (m, 4H, CH_2O), 3.92 (s, 6H, OCH_3), 1.15 (t, $^3J_{H,H}$ = 7.1 Hz, 12H, CH_3) ppm. $^{31}P\{^1H\}$ NMR (300 MHz, $CDCl_3$/CD_3OD, 2:1 v/v, 25 °C): δ 25.8 ppm. MS (MALDI-TOF): *m*/*z* calcd. for $C_{42}H_{45}N_4O_8P_2$ [M + H]$^+$ 795.3; found 795.1. UV−vis ($CHCl_3$): λ_{max} [log (ε/M^{-1} cm^{-1})] = 420 (5.34), 522 (4.16), 561 (4.26), 598 (3.96), 653 (4.24) nm.

*[5,15-Bis(diethoxyphosphoryl)-10,20-bis(4′-methoxyphenyl)porphyrinato(2−)]zinc (**3a**).* ^{1}H NMR (300 MHz, $CDCl_3$/CD_3OD, 2:1 v/v, 25 °C): δ 10.02 (d, $^3J_{H,H}$ = 4.9 Hz, 4H, Hβ), 8.69 (d, $^3J_{H,H}$ = 4.9 Hz, 4H, Hβ), 7.85 (d, $^3J_{H,H}$ = 8.5 Hz, 4H, *o*-Ph), 7.09 (d, $^3J_{H,H}$ = 8.6 Hz, 4H, *m*-Ph), 4.37−4.23 (m, 4H, CH_2O), 4.11−3.98 (m, 4H, CH_2O), 3.91 (s, 6H, OCH_3), 1.17 (t, $^3J_{H,H}$ = 7.1 Hz, 12H, CH_3) ppm. ^{13}C NMR (150 MHz, $CDCl_3$/CD_3OD (2:1), 25 °C): δ 159.35 (2C, $\underline{C}_{Ar}OCH_3$), 151.90 (d, $^2J_{C,P}$ = 2.6 Hz, 4C, α-C), 151.08 (4C, α-C), 135.33 (4C, *m*-CH_{Ar}), 135.17 (2C, $\underline{C}_{Ar}$), 133.03 (4C, β-CH), 132.71 (4C, β-CH), 122.37 (2C, *meso*-C), 111.96 (4C, *o*-CH_{Ar}), 101.99 (d, $^2J_{C,P}$ = 183 Hz, 2C, *meso*-C), 62.84 (d, $^2J_{C,P}$ = 4.7 Hz, 4C, OCH_2), 55.44 (2C, OCH_3), 16.14 ppm (d, $^3J_{C,P}$ = 6.6 Hz, 4C, $OCH_2\underline{C}H_3$). $^{31}P\{^1H\}$ NMR (300 MHz, $CDCl_3$/CD_3OD, 2:1 v/v, 25 °C): δ 27.8 ppm. HRMS (ESI): *m*/*z* calcd. for $C_{42}H_{42}N_4NaO_8P_2Zn$ [M + Na]$^+$ 879.16616; found 879.16723. IR (neat): ν 2962 (w), 2928 (w), 2830 (w), 1606 (m), 1526 (m), 1510 (m), 1474 (m), 1463 (m), 1439 (m), 1407 (m), 1389 (m), 1325 (m), 1292 (m), 1245 (s, P═O), 1222 (m), 1200 (m, P═O), 1172 (m), 1087 (m), 1033 (m), 1013 (m, P−O), 982 (s, P−O), 951 (s), 886 (s), 842 (s), 796 (s), 745 (s), 715 (m), 668 (m), 639 (m), 579 (s), 564 (s), 553 (s) cm^{-1}. UV−vis ($CHCl_3$): λ_{max} [log (ε/M^{-1} cm^{-1})] = 427 (5.45), 565 (3.92), 603 (4.35) nm.

Porphyrin **3a** was also prepared using the $Pd(OAc)_2$/PPh_3 (1/3 molar ratio) catalytic system. However, under these conditions, the product isolation was also tedious and the product yield was low. For example, the reaction carried out in the presence of 10 mol % $Pd(OAc)_2$/PPh_3 afforded **3a** in 10% yield. Attempts to simplify product isolation by using 10 mol % of the $Pd(OAc)_2$/dppf catalytic system gave only partial success because the product yield decreased to 10% owing to an acceleration of the side hydrodebromination reaction.

Synthesis of [5,15-Bis(diethoxyphosphoryl)-10,20-bis(4′-cyanophenyl)porphyrinato(2−)]zinc (3d). A two-neck round-bottom flask equipped with a reflux condenser, a magnetic stirrer bar, and a gas outlet was charged with bromoporphyrin **5d** (45.6 mg, 0.062 mmol), $Pd(OAc)_2$ (1.4 mg, 0.0062 mmol), and dppf (7 mg, 0.0125 mmol). The reaction vessel was evacuated and purged with nitrogen three times. Subsequently, 3 mL of an anhydrous toluene/ethanol mixture (1:1, v/v), diethyl H-phosphonate (3.1 mmol, 0.396 mL), and NEt_3 (0.928 mmol, 0.130 mL) were added by syringes. The reaction mixture was stirred at reflux for 3 days. The course of the reaction was monitored by MALDI-TOF and ^{1}H NMR spectroscopy. After complete conversion of dibromide **5d** and [5-bromo-15-diethoxyphosphoryl-10,20-bis(4′-cyanophenyl)porphyrinato(2−)]-zinc, the reaction mixture was allowed to cool to room temperature and concentrated under reduced pressure. The solid residue was dissolved in chloroform and subjected to column chromatography on silica gel using a $CHCl_3$/CH_3OH mixture (98:2, v/v) as eluent to afford **3d** in 71% yield (37.4 mg). ^{1}H NMR (300 MHz, $CDCl_3$/CD_3OD, 2:1 v/v, 25 °C): δ 10.10 (d, $^3J_{H,H}$ = 4.9 Hz, 4H, Hβ), 8.57 (d, $^3J_{H,H}$ = 4.9 Hz, 4H, Hβ), 8.11 and 7.90 (AB system, J_{AB} = 8.0 Hz, 8 H, *m*-Ph and *o*-Ph, respectively), 4.37−4.25 (m, 4H, CH_2O), 4.13−4.00 (m, 4H, CH_2O), 1.17 (t, $^3J_{H,H}$ = 7.1 Hz, 12H, CH_3) ppm. ^{13}C NMR (150 MHz, $CDCl_3$/CD_3OD (2:1), 25 °C): δ 152.29 (d, $^4J_{C,P}$ = 2.3 Hz, 4C, α-C), 149.83 (4C, α-C), 147.85 (2C, $\underline{C}_{Ar}$), 134.77 (4C, *m*-CH_{Ar}), 134.02 (4C, β-CH), 132.07 (4C, β-CH), 130.34 (4C, *o*-CH_{Ar}), 120.20 (2C, *meso*-C), 118.93 (2C, $\underline{C}_{Ar}$CN), 111.57 (2C, CN), 103.42 (d, $^2J_{C,P}$ = 184.5 Hz, 2C, *meso*-C), 63.05 (d, $^2J_{C,P}$ = 5.3 Hz, 4C, OCH_2), 16.18 (d, $^3J_{C,P}$ = 6.6 Hz, 4C, $OCH_2\underline{C}H_3$). $^{31}P\{^1H\}$ NMR (300 MHz, $CDCl_3$/CD_3OD, 2:1 v/v, 25 °C): δ 26.79 ppm. HRMS (ESI): *m*/*z* calcd. for $C_{42}H_{36}N_6NaO_6P_2Zn$ [M + Na]$^+$ 869.1355; found 869.13201. IR (neat): ν 2978 (w), 2925 (w), 2896 (w), 2228 (s, C≡N), 1604 (m), 1530 (m), 1475 (m), 1410 (m), 1393 (m), 1324 (w), 1221 (s), 1199 (s, P═O), 1161 (w), 1094 (m), 1083 (m), 1040 (s), 1014 (s, P−O), 981 (s, P−O), 959 (s), 939 (s), 890 (s), 868 (m), 855 (s), 804 (w), 798 (s), 745 (s), 725 (m), 712 (s), 670 (m), 667 (m), 661 (m), 647 (m), 585 (s), 564 (s), 558 (s), 551 (s) cm^{-1}. UV−vis ($CHCl_3$): λ_{max} [log (ε/M^{-1} cm^{-1})] = 426 (5.45), 563 (4.07), 602 (4.32) nm.

Porphyrin **3d** was also prepared in the presence of a 10 mol % of $Pd(OAc)_2$/PPh_3 (1/3 molar ratio) catalytic system. The product was obtained in low (15%) yield according to NMR characterization of the solid residue obtained after evaporation of the reaction mixture.

DOI: 10.1021/acs.inorgchem.9b00268
Inorg. Chem. XXXX, XXX, XXX−XXX

RESULTS AND DISCUSSION

Synthesis. The *trans*-A_2-type porphyrins **1a−d** were prepared according to the previously reported procedures (see Experimental Section). The phosphorylporphyrins **2a−d** were synthesized by Pd-catalyzed cross-coupling of the bromoporphyrins **4a−d** with diethyl H-phosphonate (Scheme 1) as earlier reported.[58]

Scheme 1. Synthesis of Diethoxyphosphorylporphyrins 2a−d and 3a−d

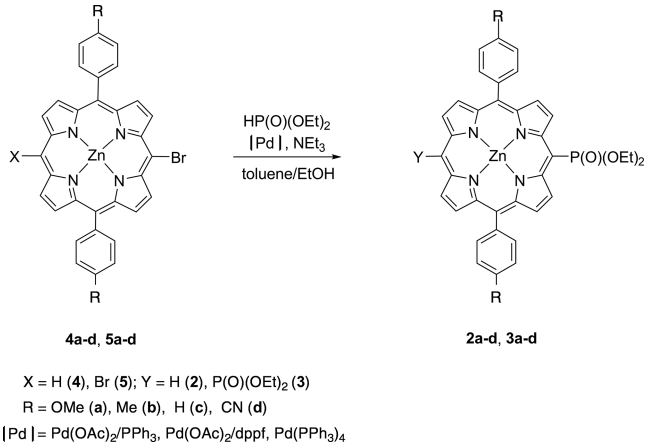

X = H (**4**), Br (**5**); Y = H (**2**), P(O)(OEt)$_2$ (**3**)
R = OMe (**a**), Me (**b**), H (**c**), CN (**d**)
[Pd] = $Pd(OAc)_2/PPh_3$, $Pd(OAc)_2$/dppf, $Pd(PPh_3)_4$

All compounds were obtained in good yield (60−85%) using triethylamine as a base in the presence of the $Pd(OAc)_2/PPh_3$ catalytic precursor.

The diphosphonates **3a−d** were first prepared from the *meso*-dibromoporphyrins **5a−d** and diethyl H-phosphonate according to a similar procedure as for monophosphorylated derivatives (Scheme 1). This synthetic approach to the diphosphonates **3b**[53] and **3c**[28] was previously reported. Unlike similarly as what was observed in the synthesis of the phosphonates **2a−d**, the product yield of **3a−d** was strongly dependent on the nature of the *meso*-aryl substituents when the $Pd(OAc)_2/PPh_3$ catalytic system was employed for phosphonylation of the dibromides **5a−d**. A good yield for **3c** (51%) was obtained only from the dibromide **5c**, whereas the yield decreased to 34% for the porphyrin **3b** and fell to 10−15% for the diphosphonate porphyrins **3a** and **3d** where the hydrodebromination reaction was predominant under these experimental conditions. Thus, an optimization of the reaction procedure was performed. It was determined that the nature of catalyst is a key parameter to increase the efficiency of this Pd-catalyzed reaction. Diphosphonate **3a** was prepared in 45% yield using $Pd(PPh_3)_4$, whereas **3d** was isolated in good yield (71%) only when this catalyst was replaced by $Pd(OAc)_2$/dppf.

It should be noted that the yield of both products **3a** and **3d** as determined by NMR was as high as 75−80%, but chromatographic purification of the porphyrin **3a** from triphenylphosphine oxide was tedious. This compound was obtained in pure form only after its transformation into the corresponding free base porphyrin, which was purified by column chromatography and then reacted with zinc acetate dihydrate to give the target product. This reaction sequence involving three column chromatography purifications led to the pure product, but in lower isolated yield.

Electrochemistry. Each zinc porphyrin in the three series was characterized by cyclic voltammetry in three nonaqueous solvents (PhCN, CH_2Cl_2, and Py) containing 0.1 M TBAP. Examples of the voltammograms obtained for compounds **2a−2d** in PhCN are illustrated in Figure 1, and the measured half-wave potentials for the first reversible reduction and two reversible oxidations in this solvent are summarized in Table 1.

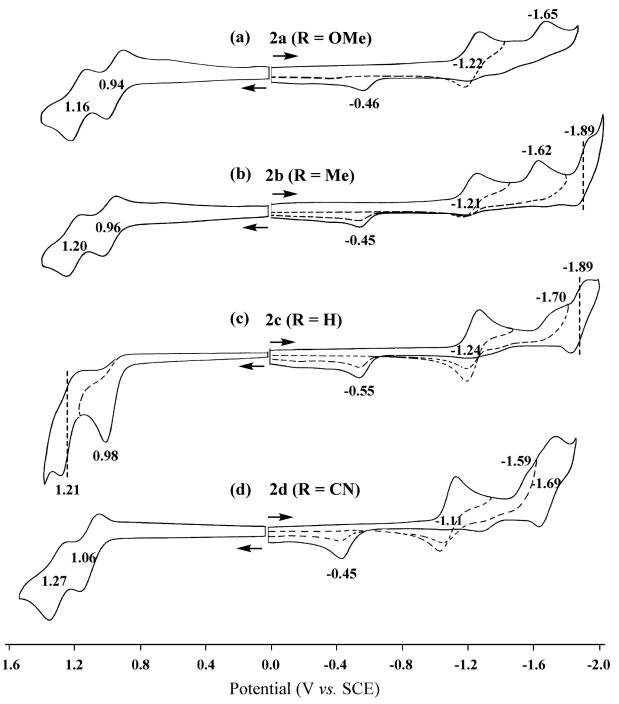

Figure 1. Cyclic voltammograms of investigated monophosphorylated porphyrins **2a−d** in PhCN containing 0.1 M TBAP.

Table 1. Half-Wave and Peak Potentials (V vs SCE) of Investigated Porphyrins in PhCN Containing 0.1 M TBAP

		oxidation		reduction	
R	Cpd	second	first	first	H-L[c]
OMe	**1a**	1.10	0.78	−1.43	2.21
	2a	1.16	0.94	−1.22	2.16
	3a	1.16	1.00	−1.01	2.01
Me	**1b**	1.11	0.79	−1.42	2.21
	2b	1.20	0.96	−1.21	2.17
	3b	1.18	1.01	−1.00	2.01
H	**1c**	1.12	0.81	−1.40	2.21
	2c	1.21	0.98[a]	−1.24	2.12
	3c[b]	1.32[a]	1.06	−0.97	2.03
CN	**1d**	1.17	0.89	−1.32	2.21
	2d	1.27	1.06	−1.11	2.17
	3d	1.27	1.13	−0.92	2.05

[a]Irreversible peak potential at a scan rate = 0.1 V/s. [b]Data taken from ref 53. [c]The HOMO−LUMO gap (V).

Not included in the table are potentials for the second or third reductions, the first of which involves a coupled chemical reaction to give a phlorin anion radical and the second a reversible one-electron reduction of this homogeneously generated product.[56]

Similar chemical reactions of the doubly reduced porphyrin are seen for the diphosphorylated derivatives **3a−3d** as shown in Figure 2 for compound **3d**. As seen in this figure, adding one

DOI: 10.1021/acs.inorgchem.9b00268
Inorg. Chem. XXXX, XXX, XXX−XXX

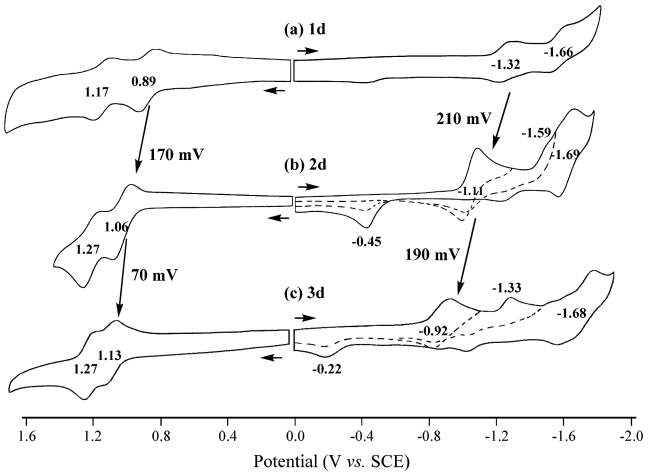

Figure 2. Cyclic voltammograms of **1d**, **2d**, and **3d** in PhCN containing 0.1 M TBAP. Scan rate = 0.1 V/s.

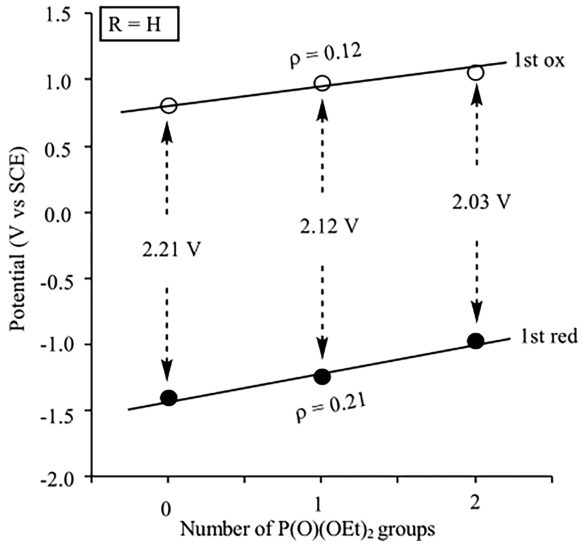

Figure 3. Correlation between number of $P(O)(OEt)_2$ groups on the porphyrin and the first reduction or oxidation of compounds **1c**, **2c**, and **3c** in PhCN, 0.1 M TBAP.

phosphoryl group to a *meso*-position of the nonphosphorylated porphyrin **1d** to give **2d** shifts of $E_{1/2}$ for the first reduction by 210 mV (from −1.32 to −1.11 V) and a further 190 mV shift toward positive potentials is seen when a second *meso*-phosphoryl group is added to the porphyrin to give compound **3d** which is reduced at −0.92 V in the first one-electron addition.

The second reduction of compounds **2d** and **3d** to form the porphyrin dianions is located at E_p = −1.59 and −1.33 V, respectively (see Figure 2), while the third reductions of these two porphyrins are assigned to reduction of the in situ generated phlorin anion radicals, reactions which occur at virtually the same half-wave potentials of −1.69 and −1.68 V. Similar reduction potentials are also seen in PhCN for the third reduction of compounds **2b** ($E_{1/2}$ = −1.89 V, Figure 1) and **3b** ($E_{1/2}$ = −1.90 V). It should also be noted that the measured shifts in the two reversible oxidation potentials are both larger upon going from compound **1d** to **2d** in PhCN (170 mV for the first oxidation and 100 mV for the second) than the shifts in $E_{1/2}$ upon going from compounds **2d** to **3d** (70 mV for the first oxidation and 0 mV for the second).

As shown in a previous publication,[56] the rate of phlorin formation decreases when changing the electrochemical solvent from CH_2Cl_2 or PhCN to a more coordinating and basic solvent such as pyridine, and this effect of solvent is also observed for the currently investigated porphyrins as shown in Table S1 and Figures S15 and S16 which compare voltammograms for the reductions of **1d**−**3d** and **2a**−**2d** in pyridine containing 0.1 M TBAP. The potentials for the first and second one-electron additions to the phosphorylated porphyrins **2d** and **3d** in pyridine are both shifted positively from **1d** due to the electron-withdrawing effect of the phosphoryl groups.

More importantly, there is much less phlorin anion formation following generation of the porphyrin dianion in the second reduction as judged by the anodic peak current on the return voltammetric scan (Figure S15).

The potentials for the first reduction and first oxidation of related porphyrins with the same set of *meso*-phenyl substituents are linearly related to the number of *meso*-$P(O)(OEt)_2$ groups on the compound as shown graphically in Figure 3 for compounds **1c**, **2c**, and **3c**. The first reduction is more affected by the number of *meso*-phosphorylated groups on the porphyrin than the first oxidation, this being seen by the slopes of the $E_{1/2}$ vs number of $P(O)(OEt)_2$ groups which are 0.21 and 0.12 V for the oxidation and reduction, respectively. Because the two slopes are not equal, the electrochemically measured HOMO−LUMO gap decreases with increase in the number of phosphoryl groups on the porphyrin, going from 2.21 V for compound **1c** to 2.03 V for compound **3c**.

Substituent Effects of the Two *meso*-Phenyl Groups. It has long been known that the addition of electron-donating or electron-withdrawing groups to the periphery of a porphyrin macrocycle will modify both the physical properties and the chemical reactivity of the compounds.[61] The effect of substituents on redox potentials for a given set of closely related compounds can generally be quantitated by the linear free energy relationship $E_{1/2} = \Sigma\sigma\rho$, where $E_{1/2}$ is the half-wave potential for each redox process of the compound, σ is the Hammett substituent constant, and ρ, measured in volts, represents the sensitivity of the given redox reaction to the change of substituents.

Figure S17 illustrates how redox potentials of the four investigated monophosphorylated porphyrins vary as a function of the phenyl ring substituents in PhCN. As shown in the figure, a linear relationship is observed for the first reduction as well as for the first and second oxidations. These three processes each involve reversible one-electron transfers in PhCN, and the 52−63 mV slopes of the $E_{1/2}$ vs σ plots are within the range observed for numerous porphyrins having *meso*-phenyl groups with electron-donating or electron-withdrawing substituents.[61]

Axial Ligand Binding by Porphyrins 2d and 3d. The self-assembly of porphyrins having a phosphoryl group has previously been demonstrated, both in the solid state and in solution.[27,31,38,62,63] This assembly results when the phosphoryl group from one porphyrin molecule axially binds to the metal center of another molecule, leading to the formation of laterally shifted cofacial dimers[29] or 1D[26] or 2D[28] polymer networks.

The axial ligand binding reaction involving the Zn(II) metal center in the associated dimers can be simulated by a titration of the phosphoryl porphyrins with Ph_3PO, and this was done in the current study for compounds **1d**, **2d** and **3d**, with the

DOI: 10.1021/acs.inorgchem.9b00268
Inorg. Chem. XXXX, XXX, XXX−XXX

process being spectroscopically monitored in a $CHCl_3$/MeOH (9:1) mixture.

A binding of Ph_3PO to the Zn(II) center of the porphyrin readily occurs, and this leads to the spectral changes illustrated in Figure 4 where the Soret band is shifted by 10 nm and the

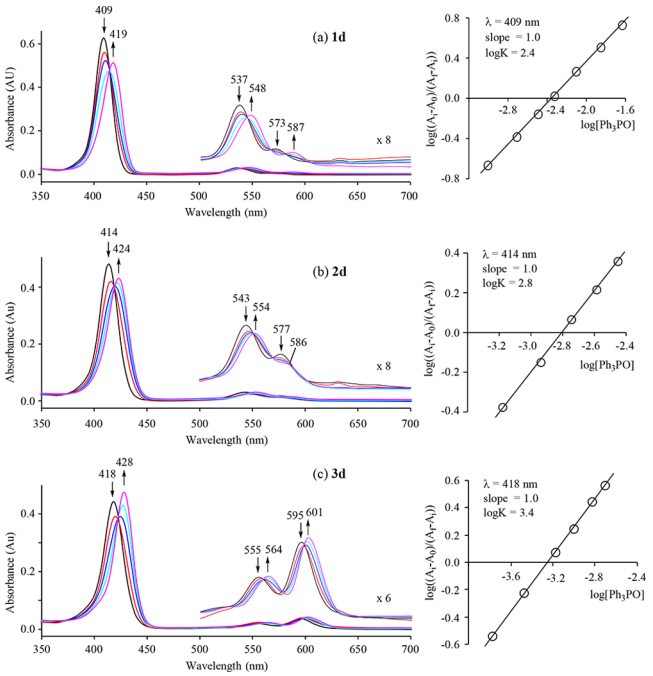

Figure 4. UV−vis spectral change of (a) **1d**, (b) **2d**, and (c) **3d** in $CHCl_3$/MeOH (9:1) upon addition of Ph_3PO (inset shows the Hill plots).

Q-band by 9−13 nm after the binding of one Ph_3PO group. Calculated equilibrium constants (log K) for the binding of one Ph_3PO molecule were 2.4, 2.8, and 3.4 for **1d**, **2d** and **3d**, respectively. This trend in log K with increase in the number of *meso*-$P(O)(OEt)_2$ substituents also follows from the ease of dimerization for the di- and monophosphorylated porphyrins as described in other sections of this paper.

Attempts to Electrochemically Detect Dimerization. A dimerization was not electrochemically observed for any of the porphyrins at room temperature as well at low temperature except for compounds **2d** and **3d** in CH_2Cl_2. For example, in the case of **3d** at room temperature, the first reduction is reversible and located at $E_{1/2}$ = −0.92 V (Figure 5a), but as the temperature is lowered, first to −25 °C and then −50 °C, the first reduction splits into two reversible processes located at $E_{1/2}$ = −0.88 and −1.03 V. Although the first reduction is split into two processes at low temperature, the second reduction remains irreversible and is located at almost the same peak potential of about −1.33 V at all temperatures, thus indicating that the chemical reaction following the second reduction is fast, even at low temperature.

It has to be noted that the decrease of temperature induced only a small change in oxidation potentials for the porphyrin **3d** where well-defined and well-separated one-electron processes were seen (figure not shown). This contrasts with previously described covalently linked cofacial porphyrin dimers which could exhibit a splitting of both the reduction and oxidation potentials.[64] Moreover, in the case of an earlier-reported laterally shifted cofacial dimer formed through coordinative bonding of a *meso*- or *β*-pyrrolic dialkoxyphosphoryl group to the Zn(II) center of another molecule, only a splitting of the first oxidation potential was observed.[27,54] Thus, the behavior of the currently examined self-assembled dimer $(\mathbf{3d})_2$ is unusual and might result from the presence of two strong electron-withdrawing diethoxyphosphoryl substituents on the porphyrin macrocycle. Indeed, these substituents should favor a stabilization of the dimeric anion radical but induce a dissociation of the corresponding cation radical dimer formed in the oxidation. Similar electrochemical behavior was previously reported for compound **3b** by our lab,[53] but a splitting of the first reduction wave for this compound was

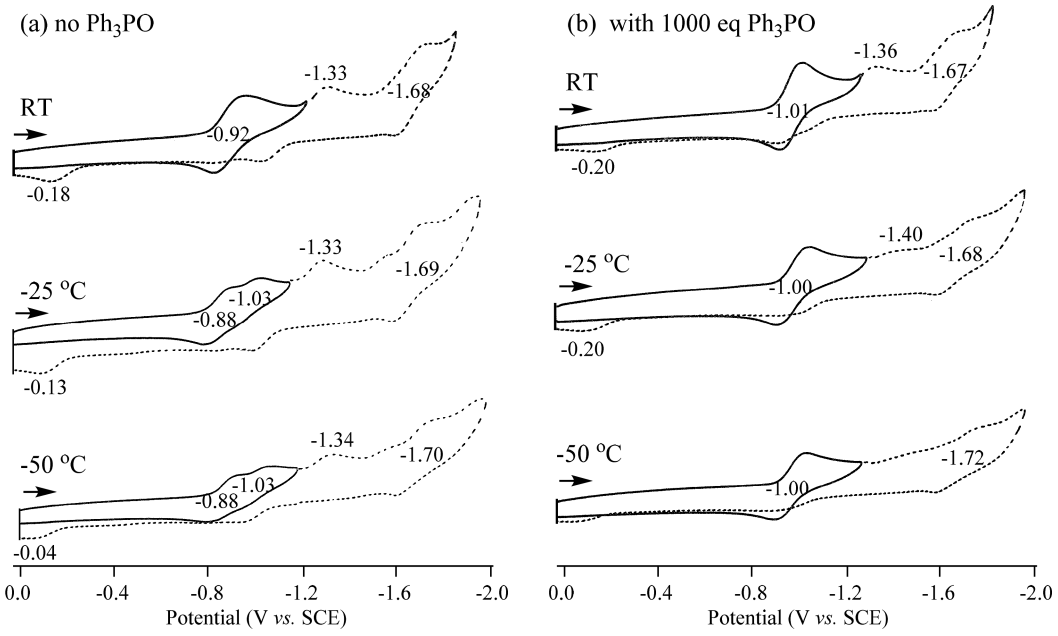

Figure 5. Cyclic voltammograms of **3d** in CH_2Cl_2 at different temperatures before (a) and after (b) addition of 1000 equiv of triphenylphosphine oxide (Ph_3PO).

DOI: 10.1021/acs.inorgchem.9b00268
Inorg. Chem. XXXX, XXX, XXX−XXX

Scheme 2. Conversion between Monomeric and Aggregated Redox Active Forms of Porphyrin 3d in CH_2Cl_2 Solution

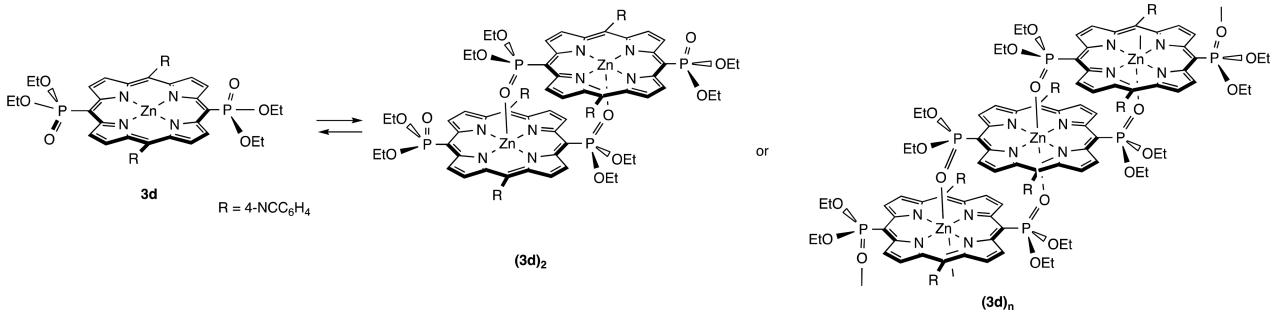

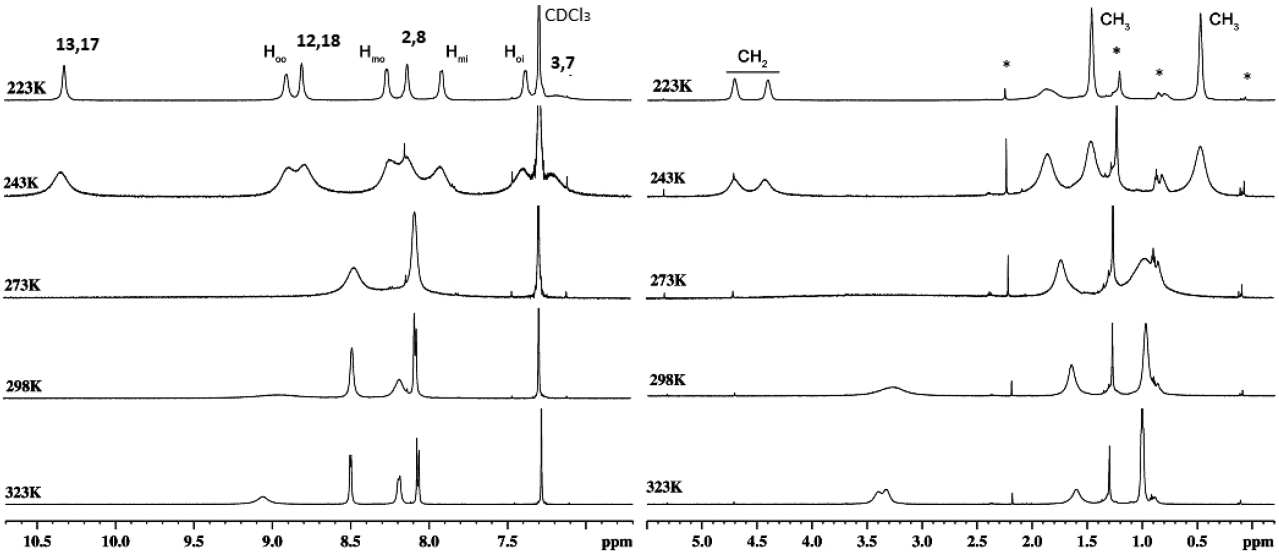

Figure 6. ^{1}H VT-NMR spectra of **3d** in $CDCl_3$ at 223−323 K. Stars correspond to the signals of impurities.

much less pronounced as compared to the porphyrin **3d** which contains four electron-withdrawing *meso*-substituents, two of $P(O)(OEt)_2$ and two of PhCN.

Cyclic voltammograms of **3d** obtained in CH_2Cl_2 containing 1000 equiv of Ph_3PO are also shown in Figure 5b and demonstrate that the first reduction involves a reversible one-electron transfer at all temperatures from RT to −50 °C. This is because the porphyrin Zn(II) center is coordinated to the added Ph_3PO axial ligand which prevents self-association.

In summary, two redox active forms of compound **3d** are proposed to exist in the CH_2Cl_2 solution under the electrochemical conditions (Scheme 2). One is a dimer or higher aggregate ($(\mathbf{3d})_n$ is shown as an example in Scheme 2), which is reduced at −1.03 V at temperatures between −25 and −50 °C, and the other is a monomer which is reduced at $E_{1/2}$ = −0.88 V at LT and at −0.92 V at RT as seen in Scheme 2.

The potential for reduction of $(\mathbf{3d})_2$ (or $(\mathbf{3d})_n$) is the same as for the reversible one-electron reduction of the monomer when complexed with Ph_3PO ($E_{1/2}$ = −1.01 V). This result is consistent with similar binding constants for complexation of the Zn(II) center in one molecule of **3d** with a $P(O)(OEt)_2$ group from another porphyrin molecule or Ph_3PO, when added to a CH_2Cl_2 solution of the compound.

The fact that monomeric **3d** is electrochemically easier to reduce than the higher aggregate by 150 mV in CH_2Cl_2 would thus favor a shift of equilibrium shown in Scheme 2 to its more easily reducible monomeric form at the electrode surface under the application of an applied potential (during the negative potential scan). Moreover, if the rate of conversion between the two forms of the porphyrin were sufficiently fast at room temperature, only the monomer redox processes would be electrochemically detected, thus giving the "false impression" that only monomers existed in solution, despite strong spectral and structural evidence to the contrary (see following sections of the paper).

A similar temperature dependent equilibrium between two forms of the redox active species is also seen for the monophosphoryl porphyrin **2d** as shown in Figure S18, but lower temperatures are needed in order to observe split redox processes during the electroreduction in CH_2Cl_2. For example, no splitting of reduction potentials is observed at −35 °C for porphyrin **2d**, but a split process starts to be seen at −60 °C as illustrated in Figure S18. Again, like in the case of compound **3d**, only a single well-defined reduction is observed after addition of 1000 equiv of Ph_3PO to the solution where only monoligated Ph_3PO monomers are present and the reversible reduction potential under these conditions (−1.31 V) is virtually the same as the potential for reduction of the higher aggregate at LT (−1.32 V). Also like in the case of **3d**, the difference in reduction potential between the monomer and the aggregate amounts to 150 mV, thus leading again to formation of the more easily reducible monomer at the electrode surface during the negative potential scan.

^{1}H and ^{31}P{^{1}H} NMR Studies of Self-Assembly in Solution. To gain a deeper insight into the structure and stability of the self-assembled species formed in solution of the

DOI: 10.1021/acs.inorgchem.9b00268
Inorg. Chem. XXXX, XXX, XXX−XXX

phosphorylporphyrin **3d**, this complex was investigated by ^{1}H and $^{31}P\{^{1}H\}$ NMR spectroscopy.

A well-resolved ^{1}H NMR spectrum of porphyrin **3d** was obtained in a $CDCl_3/CD_3OD$ (5:1, v/v) mixture at 323 K (Figure S19a). Four signals were observed in the aromatic region as expected for [5,15-bis(diethoxyphosphoryl)-10,20-bis(4′-R-phenyl)porphyrinatozinc exhibiting C_{2v} symmetry, and this indicated the presence of a monomer species **3d** in the studied solution. In contrast, when **3d** was dissolved in $CDCl_3$ (10^{-4}–10^{-2} M) at 298–323 K, the ^{1}H NMR spectrum was broadened and the data could not be used for structural analysis (Figure S19a). However, when CD_3OD was gradually added to this solution, all broadened signals of the β-pyrrolic and methylene protons shifted downfield and narrowed (Figure S19c,d). This is a typical spectral behavior for self-assembled phosphorylporphyrins and results when replacement of the coordinated phosphonate group by methanol molecules in the coordination sphere of the Zn(II) ions occurs, thus suppressing the coordination-driven self-assembly of the porphyrin molecules.[28]

Variable-temperature NMR (VT-NMR) studies (223–323 K) of **3d** in $CDCl_3$ provide important structural information because the temperature variation significantly influences the association process. The ^{1}H and $^{31}P\{^{1}H\}$ VT-NMR spectra are shown in Figures 6 and 7, respectively.

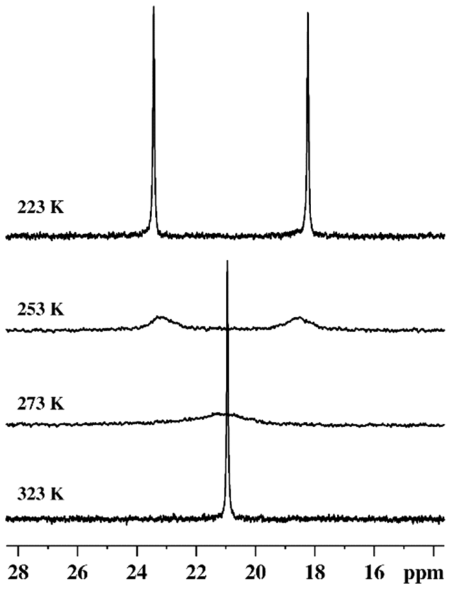

Figure 7. $^{31}P\{^{1}H\}$ VT-NMR spectra of **3d** in $CDCl_3$ at 223–323 K.

A decrease of the temperature to 223 K led to resolved ^{1}H and $^{31}P\{^{1}H\}$ NMR spectra which perfectly correspond to the spectra expected for a laterally shifted cofacial dimer $(\mathbf{3d})_2$ (Scheme 2). Indeed, the $^{31}P\{^{1}H\}$ NMR spectrum at 223 K showed two phosphorus signals ($\Delta\delta_P$ 5.26 ppm) (Figure 7). The upfield signal (δ_P 18.19 ppm) was assigned to the phosphonate group coordinated to the Zn(II) center (P_c) which was subjected to the shielding effect of the porphyrin π system. A set of proton signals characteristic for a centrosymmetric porphyrin species with nonequivalent protons of *meso*-aryl substituents also appeared in the aromatic region of the ^{1}H NMR spectrum (Figure 6).

All proton signals were assigned on the basis of chemical shifts, relative intensities, and cross-peaks in the ^{1}H–^{1}H COSY map (Figure S21). The signals of the 3,7- and 2,8-β-protons were upshifted to δ_H 7.15 and 8.13 ppm, respectively (for the numbering, see Chart 2) due to the shielding effect of the porphyrin ring current on the β-pyrrolic protons in the vicinity of the coordination site.

Chart 2. Numbering of Protons in Dimer $(\mathbf{3d})_2$

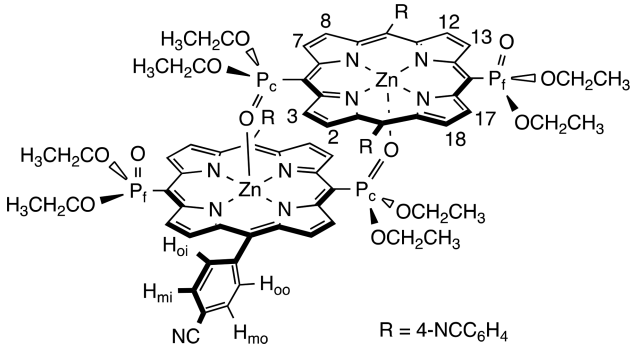

The other signals of the macrocycles observed at δ_H 8.73 and 10.29 ppm can be assigned to protons of the two pyrrole rings adjacent to the noncoordinated (free) phosphonate group (P_f) (12,18 and 13,17, respectively). The shielding of the peripheral β-protons upon going from a dimer $(\mathbf{3d})_2$ to the reference monomer species in a $CDCl_3/CD_3OD$ mixture increases in the order 13,17 ($\Delta\delta_H$ = 0 ppm) < 2,8 ($\Delta\delta_H$ = 0.65 ppm) < 3,7 ($\Delta\delta_H$ = 3.14 ppm). These values perfectly correspond to resonances observed for similar cofacial dimers formed by 5-di-*n*-butoxyphosphoryl-10,15,20-tris(3′,5′-di-*tert*-butylphenyl)porphyrinatozinc (**6**) (Chart 3, Figure S24).[27]

Chart 3. Structure of Previously Reported Porphyrins Displaying Self-Organization in Crystals and in Solutions

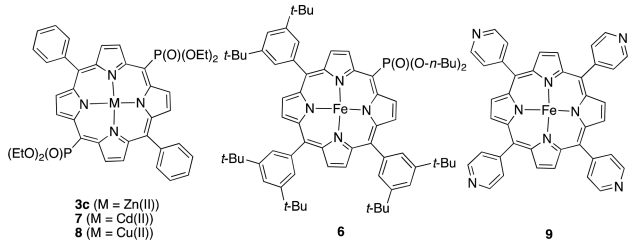

The protons 12 and 8 are somewhat deshielded ($\Delta\delta_H$ = 0.08 ppm) relative to the corresponding signal for the reference monomer **3d**. This is in contrast to the change observed for the dimer $(\mathbf{6})_2$ in which these protons are shifted upfield ($\Delta\delta_H$ = −0.05 ppm) compared to the signal of the monomeric species **6**. This inconsistency may reflect a difference in the orientation of the aryl substituents with respect to the macrocyclic plane of the dimer $(\mathbf{3d})_2$ and the sterically hindered complex $(\mathbf{6})_2$.

The set of ^{1}H NMR signals for the two diethoxyphosphoryl groups are still broadened at 223 K, but their spectral patterns are typical for a laterally shifted cofacial dimer. Diastereotopic methylene protons of the free diethoxyphosphoryl group (P_f) appear as two broad singlets at δ_H 4.68 and 4.39 ppm. The methylene signals of the coordinated phosphorus substituent (P_c) are overlapped with a broad signal of water molecules as indicated by ^{1}H–^{1}H COSY NMR experiments. The methyl protons of the P_f and P_c diethoxyphosphoryl groups appear as two broad singlets at δ_H 1.46 and 0.47 ppm, respectively.

DOI: 10.1021/acs.inorgchem.9b00268
Inorg. Chem. XXXX, XXX, XXX–XXX

Raising the temperature from 223 to 293 K leads to the pairwise coalescence of the signals belonging to the inward- and outward-oriented *ortho* and *meta* protons of the aryl substituents, as well as of two pairs of *β*-pyrrolic protons. The signals of the ethoxy groups of the two phosphorus substituents P_c and P_f are also gradually shifted toward each other and their coalescences are observed at 273−278 K. The symmetry of the porphyrin species present in the solution at 323 K is similar to that of the monomer **3d**. However, chemical shifts of all protons and particularly those of the 3,7-*β* and methylene groups are different from the corresponding signals of the reference monomer **3d** in $CDCl_3$/MeOH-*d*4 (99:1) ($\Delta\delta_H$ = 1.23 and 0.97 ppm, respectively). This indicates that the self-assembly of complex **3d** still persists in the studied solution and the observed spectral pattern reflects a rapid exchange of porphyrin molecules in the self-assembled system $(\mathbf{3d})_2$ (Scheme 2).

When comparing the corresponding proton signals of **3d** in $CDCl_3$ at 273−323 K with signals of the dimer $(\mathbf{3d})_2$ at 223 K and those of the monomer **3d** in the $CDCl_3$/MeOH-*d*4 (99:1) mixture at 273−323 K (Figure S22), it can be concluded that the molar fraction of the monomeric species is small in the studied solution. Indeed, the expected chemical shifts for the dimeric species exhibiting a rapid exchange of porphyrin molecules (the midpoint between the two pairwise signals at 223 K; for example, 2,8- and 12,18-*β*-protons) are very close to those observed in the spectra at 273−323 K, with the only exception being the 3,7-*β*-proton shift. These protons appear at δ_H = 9.09 ppm at 323 K, whereas the calculated value of their chemical shift is δ_H = 8.65 ppm. It seems likely that the signals of the 3,7-*β*-pyrrolic protons are much more temperature-dependent than those of the other protons due to the presence of the adjacent phosphonate group which exhibits weak conjugative d*π*−p*π* interactions,[65] magnetic anisotropy, and hydrogen bonding[62] with these protons. The ^{1}H VT-NMR spectrum of the reference monomer **3d** recorded in $CDCl_3$/CD_3OD (5:1) is in accordance with this hypothesis (Figure S22).

$^{31}P\{^1H\}$ VT-NMR data obtained for a $CDCl_3$ solution of porphyrin **3d** are in agreement with the formation of the fluxional dimer $(\mathbf{3d})_2$. Raising the temperature from 223 to 323 K results in a rapid positional exchange between P_c and P_f so that the corresponding signals coalesce at 273 K, giving a broad peak at δ_P 20.94 ppm.

The dimerization of porphyrin **3d** in a $CDCl_3$ solution even at a high temperature of 323 K was also confirmed by diffusion ordered spectroscopy (DOSY) data which are presented in Table S2 and Figure S23. The observed difference between the diffusion coefficients of **3d** in $CDCl_3$ and $CDCl_3/CD_3OD$ (10:1) is consistent with a 2-fold decrease in the molecular weight of **3d** upon going from the solution in $CDCl_3$ to the solution in $CDCl_3$/MeOH-*d*4.

Crystal Structure of Porphyrin 3d. Single crystals of **3d** were grown by slow diffusion of a heptane solution of this porphyrin in a $CHCl_3$/methanol mixture (97:3, v/v). X-ray analysis of the obtained crystals revealed that porphyrin **3d** displays a 2D polymer structure, being crystallized under these conditions.

In the centrosymmetric molecule of **3d**, the zinc atom is bonded to four nitrogen donor atoms of the macrocycle pyrrole moieties (Zn−N = 2.0375(8)−2.0456(10) Å) and is located in the N_4 plane (Figure 8 and Figure S25).

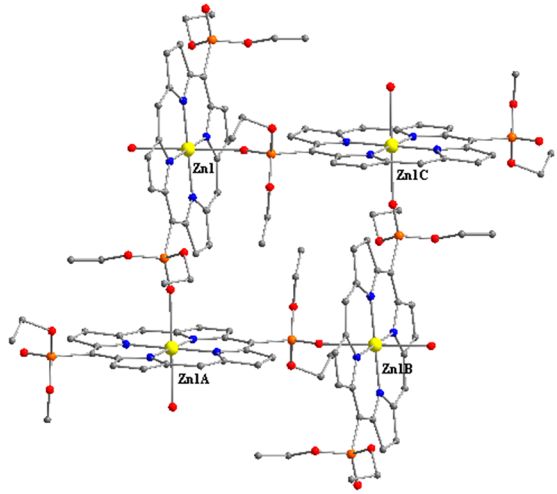

Figure 8. Primary structural unit of 2D polymer $(\mathbf{3d})_n \cdot (\mathbf{0.5\ CHCl_3})_n$ formed through the axial Zn···O═P coordination (view along the *a* axis). Hydrogen atoms and chloroform molecules are omitted for clarity.

The porphyrin macrocycle is almost planar, and the maximum deviation of carbon atoms from the ZnN_4 plane is ±0.228 Å, which is observed for the C8 and C8A atoms. The twist angles of the aryl rings with respect to the ZnN_4 plane group results from an axial coordination of its oxygen atom to the Zn(II) center of a neighboring molecule and hydrogen bonding between this atom and the *β*-pyrrolic proton of the same macrocycle. This spatial orientation of the diethoxyphosphoryl group and the porphyrin macrocycle is typical for metal complexes of porphyrins bearing a *meso*-diethoxyphosphoryl substituent directly attached to the macrocycle and was earlier observed in nickel(II), copper(II), and palladium(II) complexes having noncoordinated phosphorus substituents as well as in self-assembled associates of zinc phosphorylporphyrinates and 1D polymers where the diethoxyphosphoryl groups are coordinated to external metal ions.[55,62,63]

The metal atom of **3d** has a distorted octahedral geometry and is axially bonded with two phosphorus substituents (Figure 8). The Zn−O distance is equal to 2.4346(10) Å. This coordination bonding leads to the formation of 2D polymer in which the primary subunit can be described as a rhombus relying on four neighboring zinc atoms and having a side length of 8.360 Å and an inside angle of 84.3°. This arrangement gives rise to a two-dimensional paddle-wheel-like structure in which all metal atoms of the layer are located in the same plane with a layer depth of 15.5 Å. These layers are separated one from another by pendant aryl substituents with the distance between the nearest zinc atoms belonging to adjacent layers being 16.454 Å (Figure 9).

Distorted chloroform molecules fill a space between the aryl groups of two adjacent porphyrin layers, forming numerous short contacts with the macrocyclic scaffold and the aryl substituents.

It should be noted that Zn(II), Cd(II), and Cu(II) 5,10-bis(diethoxyphosphoryl)-10,20-diphenylporphyrins (**3c**, **7**, and **8**)[28,62,63] as well as an Fe(II) 5,10,15,20-tetra(4′-pyridyl)-porphyrin (**9**)[66] (Chart 3) also exhibit 2D polymer structures in the crystalline phase.

Despite the significant structural difference between diethoxyphosphoryl and pyridyl groups, all of the 2D coordination polymers are formed by paddle-wheel-like layers.

DOI: 10.1021/acs.inorgchem.9b00268
Inorg. Chem. XXXX, XXX, XXX−XXX

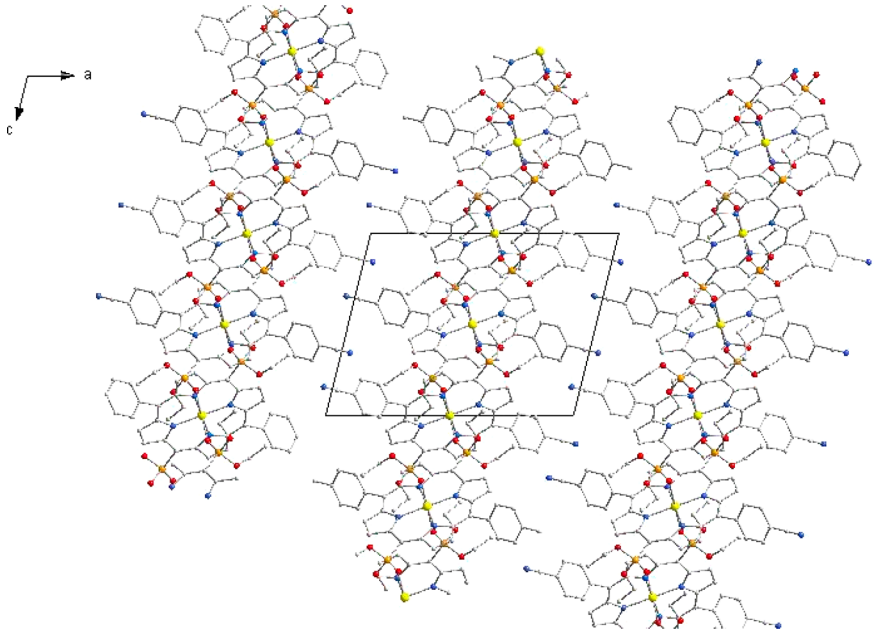

Figure 9. Spatial arrangement of layers in $(\mathbf{3d})_n \cdot (\mathbf{0.5\ CHCl_3})_n$ viewed along the b axis. Hydrogen atoms and chloroform molecules are omitted for clarity.

The difference in orientation of the electron pair of the donor groups with respect to the macrocycle axes in the pyridyl- and diethoxyphosphoryl-substituted porphyrins induces only a small distortion in spatial orientation of adjacent molecules which leads to the formation of rhombus primary subunits with an inside angle of 84.3−87.8° in the phosphorus(V)-containing polymers $(\mathbf{3c,d})_n$, $(\mathbf{7})_n$, and $(\mathbf{8})_n$. In contrast, the arrangement of the porphyrin layers is strongly influenced by both the nature of the coordinating group and aryl substituents of the macrocycle. Dense structures were obtained for two polymorphs of the 2D polymer $(\mathbf{9})_n$ and phosphorylporphyrins $(\mathbf{3c})_n$, $(\mathbf{7})_n$, and $(\mathbf{8})_n$, whereas introduction of a cyano substituent at the *meso*-aryl group of the porphyrin leads to formation of the chloroform solvated complex $(\mathbf{3d \cdot 0.5\ CHCl_3})_n$.

The switching from a 2D polymer network observed in crystals of the porphyrin **3d** to a dimeric structure after dissolving of this porphyrin in $CDCl_3$ is remarkable. To our knowledge, examples of self-assembled porphyrins exhibiting different supramolecular structures are limited to two complementary porphyrins bearing nitrogen donor sites. Dynamic equilibrium between a self-assembled trimer and tetramer of Co(III) 1-methyl-5-imidazolylporphyrin in different solvents was described by Kobuke and co-workers.[67] Another interesting example is Zn(II) 5-(4′-pyridyl)-10,15,20-triphenylporphyrinate, which displays a 1D polymer structure in crystals but seems to form discrete tetramers in solution.[68−70]

CONCLUSION

The electrochemical and spectroscopic properties for a series of zinc porphyrins **2a−d** and **3a−d** bearing the diethoxyphosphoryl group at one or two *meso*-positions of the porphyrin macrocycle were investigated. A systematic study of these compounds with comparison to the same compounds lacking these *meso*-substituents leads to a better understanding of the *meso*-(diethoxyphosphoryl)porphyrin redox properties. The first reduction of these compounds is ring-centered and leads to formation of a porphyrin π-anion radical, while the second reduction generates an unstable porphyrin dianion which undergoes a fast chemical reaction in PhCN or CH_2Cl_2 to form a phlorin anion radical. The electrochemically measured HOMO−LUMO gap decreases with an increase in the number of phosphoryl groups, and the redox potentials also vary as a function of the phenyl ring substituents as evidenced by plots of $E_{1/2}$ vs the Hammett substituent constants for groups on the two *meso*-phenyl units of the compounds.

An equilibrium between a monomeric and aggregated redox active forms of compounds **2d** and **3d** is shown to exist in CH_2Cl_2 solutions under the electrochemical conditions. Such an equilibrium was previously shown to be concentration dependent for related porphyrins, and this equilibrium is also dependent upon temperature as shown in the present study. The rate of conversion of the aggregated porphyrins **2d** and **3d** to their more easily reducible monomeric form appears to be sufficiently high at room temperature to suggest only monomers in solution, but this is not the case at LT where the rate of dissociation is sufficiently slowed down so that both forms of the redox active porphyrins can then be electrochemically detected during reduction.

To gain a deeper insight into the structure of the associates, the structure of the self-assembled supramolecular system(s) forming by zinc porphyrin **3d** was also investigated by X-ray diffraction structural analysis in the solid state and NMR spectroscopy in $CDCl_3$ solutions. Coordination of one phosphonate group to the metal center of another porphyrin molecule leads to formation of a laterally shifted cofacial dimer $(\mathbf{3d})_2$ when the compound **3d** is dissolved in chloroform, a solvent not so different from CH_2Cl_2 used for electrochemistry. In contrast to earlier-reported analogous self-assembled dialkoxyphosphorylporphyrin dimers such as $(\mathbf{6})_2$, the dimer $(\mathbf{3d})_2$ is stable at room temperature and exhibits a fluxional behavior. A rapid exchange of porphyrin molecules in the dimer $(\mathbf{3d})_2$ is observed at room temperature on the NMR time scale. In the crystalline phase, this compound displays a

DOI: 10.1021/acs.inorgchem.9b00268
Inorg. Chem. XXXX, XXX, XXX−XXX

2D polymer network formed through the coordination of Zn(II) centers by two phosphoryl groups belonging to adjacent porphyrin molecules. Accordingly, in the solid phase, both phosphonate groups of each porphyrin molecule are ligated with adjacent Zn(II) centers.

The reported data indicate that structural organization of the phosphorylporphyrins strongly depends upon the environmental conditions, and these compounds are of interest for better understanding the role of structural parameters on self-assembly of the natural tetrapyrrolic systems.

Finally, the coordination self-assembly of electron-deficient porphyrins could be electrochemically observed by the presence of a temperature dependent splitting of their first reduction potential. Thus, electrochemical characterization might in the future provide a roadmap for the rational design of self-assembled phosphorylporphyrin systems, as described in the present paper for the self-assembly of Zn(II) porphyrin **3d**.

■ ASSOCIATED CONTENT

Supporting Information

The Supporting Information is available free of charge on the ACS Publications website at DOI: 10.1021/acs.inorgchem.9b00268.

Crystallographic information, Tables S1−S3, and Figures S1−S28 (PDF)

Accession Codes

CCDC 1890813 contains the supplementary crystallographic data for this paper. These data can be obtained free of charge via www.ccdc.cam.ac.uk/data_request/cif, or by emailing data_request@ccdc.cam.ac.uk, or by contacting The Cambridge Crystallographic Data Centre, 12 Union Road, Cambridge CB2 1EZ, UK; fax: +44 1223 336033.

■ AUTHOR INFORMATION

Corresponding Authors

*E-mail: kkadish@uh.edu. Phone: (+1) 713-743-2740 (K.M.K.).

*E-mail: Alla.Lemeune@u-bourgogne.fr. Phone: (+33) (0)3-80-39-61-26 (A.B.-L.).

ORCID

Karl M. Kadish: 0000-0003-4586-6732

Yulia G. Gorbunova: 0000-0002-2333-4033

Alla Bessmertnykh-Lemeune: 0000-0001-6707-6868

Roger Guilard: 0000-0001-7328-3695

Notes

The authors declare no competing financial interest.

■ ACKNOWLEDGMENTS

We gratefully acknowledge support from the Robert A. Welch Foundation (K.M.K., Grant E-680) and the French-Russian Associated Laboratory "LAMREM" supported by the CNRS and Russian Academy of Sciences, Russian Foundation for Basic Research (Grant no. 17-53-16028). The authors thank Dr. K. Birin for helpful discussions on NMR experiences.

■ REFERENCES

(1) Wilson, M. T.; Reeder, B. J. Oxygen binding haem proteins. *Exp. Physiol.* **2008**, *93* (1), 128−132.

(2) Meunier, B. Metalloporphyrins as versatile catalysts for oxidation reactions and oxidative DNA cleavage. *Chem. Rev.* **1992**, *92* (6), 1411−1456.

(3) Denisov, I. G.; Makris, T. M.; Sligar, S. G.; Schlichting, I. Structure and chemistry of cytochrome P450. *Chem. Rev.* **2005**, *105* (6), 2253−2278.

(4) Kruse, O.; Rupprecht, J.; Mussgnug, J. H.; Dismukes, G. C.; Hankamer, B. Photosynthesis: A blueprint for solar energy capture and biohydrogen production technologies. *Photochem. Photobiol. Sci.* **2005**, *4* (12), 957−970.

(5) Balaban, T. S. Self-assembling porphyrins and chlorins as synthetic mimics of the chlorosomal bacteriochlorophylls. In *Handbook of Porphyrin Science*; Kadish, K. M., Smith, K. M., Guilard, R., Eds.; World Scientific: Singapore, 2010; Vol. *1*, pp 221−306.

(6) Morisue, M.; Kobuke, Y. Supramolecular organization of porphyrins and phthalocyanines by use of biomimetic coordination methodology. In *Handbook of Porphyrin Science*; Kadish, K. M., Smith, K. M., Guilard, R., Eds.; World Scientific: Singapore, 2014; Vol. *32*, pp 1−126.

(7) Tamiaki, H.; Kunieda, M. Photochemistry of chlorophylls and their synthetic analogs. In *Handbook of Porphyrin Science*; Kadish, K. M., Smith, K. M., Guilard, R., Eds.; World Scientific: Singapore, 2011; Vol. *11*, pp 223−290.

(8) Bessmertnykh-Lemeune, A. G.; Stern, C.; Guilard, R.; Enakieva, Y. Y.; Gorbunova, Y. G.; Tsivadze, A. Y.; Nefedov, S. E. Biomimetic studies of porphyrin self-assembled systems. In *Supramolecular Systems: Chemistry, Types and Applications*; Nova Science Publishers: Hauppauge, NY, 2016; pp 213−278.

(9) Barber, J. Photosynthetic energy conversion: natural and artificial. *Chem. Soc. Rev.* **2009**, *38* (1), 185−196.

(10) Meunier, B.; de Visser, S. P.; Shaik, S. Mechanism of oxidation reactions catalyzed by cytochrome P450 enzymes. *Chem. Rev.* **2004**, *104* (9), 3947−3980.

(11) Che, C.-M.; Lo, V. K.-Y.; Zhou, C.-Y.; Huang, J.-S. Selective functionalisation of saturated C-H bonds with metalloporphyrin catalysts. *Chem. Soc. Rev.* **2011**, *40* (4), 1950−1975.

(12) Liu, W.; Groves, J. T. Manganese catalyzed C−H halogenation. *Acc. Chem. Res.* **2015**, *48* (6), 1727−1735.

(13) Medforth, C. J.; Wang, Z.; Martin, K. E.; Song, Y.; Jacobsen, J. L.; Shelnutt, J. A. Self-assembled porphyrin nanostructures. *Chem. Commun.* **2009**, No. 47, 7261−7277.

(14) See, for example: *The Porphyrin Handbook*; Kadish, K. M., Smith, K. M., Guilard, R., Eds.; Academic Press: San Diego, CA, 2006; Vols. *1*−*20* and the references therein.

(15) Sharman, W. M.; Van Lier, J. E. Use of palladium catalysis in the synthesis of novel porphyrins and phthalocyanines. *J. Porphyrins Phthalocyanines* **2000**, *04* (05), 441−453.

(16) Setsune, J.-i. Palladium chemistry in recent porphyrin research. *J. Porphyrins Phthalocyanines* **2004**, *08* (01), 93−102.

(17) Liu, C.; Chen, Q.-Y. General and efficient synthesis of *meso*-A and *β*-perfluoroalkylated porphyrins via Pd-catalyzed cross-coupling reaction. *Synlett* **2005**, *2005* (8), 1306−1310.

(18) Takanami, T.; Hayashi, M.; Chijimatsu, H.; Inoue, W.; Suda, K. Palladium-catalyzed cyanation of porphyrins utilizing cyanoethylzinc bromide as an efficient cyanide ion source. *Org. Lett.* **2005**, *7* (18), 3937−3940.

(19) Bringmann, G.; Rüdenauer, S.; Götz, D. C. G.; Gulder, T. A. M.; Reichert, M. Axially chiral directly linked bisporphyrins: Synthesis and stereostructure. *Org. Lett.* **2006**, *8* (21), 4743−4746.

(20) Esdaile, L. J.; Senge, M. O.; Arnold, D. P. New palladium catalysed reactions of bromoporphyrins: Synthesis and crystal structures of nickel(II) complexes of primary 5-aminoporphyrin, 5,5′-bis(porphyrinyl) secondary amine, and 5-hydroxyporphyrin. *Chem. Commun.* **2006**, No. 40, 4192−4194.

(21) Tremblay-Morin, J.-P.; Ali, H.; van Lier, J. E. Palladium catalyzed coupling reactions of cationic porphyrins with organoboranes (Suzuki) and alkenes (Heck). *Tetrahedron Lett.* **2006**, *47* (18), 3043−3046.

(22) Liu, C.; Shen, D.-M.; Chen, Q.-Y. Practical and efficient synthesis of various *meso*-functionalized porphyrins via simple ligand-

DOI: 10.1021/acs.inorgchem.9b00268
Inorg. Chem. XXXX, XXX, XXX−XXX

free nickel-catalyzed C-O, C-N, and C-C cross-coupling reactions. *J. Org. Chem.* **2007**, *72* (8), 2732−2736.
(23) Beyler, M.; Beemelmanns, C.; Heitz, V.; Sauvage, J.-P. Various synthetic routes to a gable-like bis(porphyrin) constructed on a 1,10-phenanthroline chelate. *Eur. J. Org. Chem.* **2009**, *2009* (17), 2801−2805.
(24) Filatov, M. A.; Guilard, R.; Harvey, P. D. Selective stepwise Suzuki cross-coupling reaction for the modelling of photosynthetic donor-acceptor systems. *Org. Lett.* **2010**, *12* (1), 196−199.
(25) Atefi, F.; McMurtrie, J. C.; Arnold, D. P. Multiporphyrin coordination arrays based on complexation of magnesium(II) porphyrins with porphyrinylphosphine oxides. *Dalton Trans.* **2007**, No. 21, 2163−2170.
(26) Atefi, F.; McMurtrie, J. C.; Turner, P.; Duriska, M.; Arnold, D. P. *meso*-Porphyrinylphosphine oxides: Mono- and bidentate ligands for supramolecular chemistry and the crystal structures of monomeric {[10,20-diphenylporphyrinatonickel(II)-5,15-diyl]-bis-[$P(O)Ph_2$] and polymeric self-coordinated {[10,20-diphenylporphyrinatozinc-(II)-5,15-diyl]-bis-[$P(O)Ph_2$]}. *Inorg. Chem.* **2006**, *45* (16), 6479−6489.
(27) Matano, Y.; Matsumoto, K.; Terasaka, Y.; Hotta, H.; Araki, Y.; Ito, O.; Shiro, M.; Sasamori, T.; Tokitoh, N.; Imahori, H. Synthesis, structures, and properties of *meso*-phosphorylporphyrins: Self-organization through P-oxo-zinc coordination. *Chem. - Eur. J.* **2007**, *13* (3), 891−901.
(28) Enakieva, Y. Y.; Bessmertnykh, A. G.; Gorbunova, Y. G.; Stern, C.; Rousselin, Y.; Tsivadze, A. Y.; Guilard, R. Synthesis of *meso*-polyphosphorylporphyrins and example of self-assembling. *Org. Lett.* **2009**, *11* (17), 3842−3845.
(29) Vinogradova, E. V.; Enakieva, Y. Y.; Nefedov, S. E.; Birin, K. P.; Tsivadze, A. Y.; Gorbunova, Y. G.; Bessmertnykh Lemeune, A. G.; Stern, C.; Guilard, R. Synthesis and self-organization of zinc (dialkoxyphosphoryl)porphyrins in the solid state and in solution. *Chem. - Eur. J.* **2012**, *18* (47), 15092−15104.
(30) Lemeune, A.; Mitrofanov, A. Y.; Rousselin, Y.; Stern, C.; Guilard, R.; Enakieva, Y. Y.; Gorbunova, Y. G.; Nefedov, S. E. Supramolecular architectures based on phosphonic acid diesters. *Phosphorus, Sulfur Silicon Relat. Elem.* **2015**, *190* (5−6), 831−836.
(31) Enakieva, Y. Y.; Volostnykh, M. V.; Nefedov, S. E.; Kirakosyan, G. A.; Gorbunova, Y. G.; Tsivadze, A. Y.; Bessmertnykh-Lemeune, A. G.; Stern, C.; Guilard, R. Gallium(III) and indium(III) complexes with *meso*-monophosphorylated porphyrins: Synthesis and structure. A first example of dimers formed by the self-assembly of *meso*-porphyrinylphosphonic acid monoester. *Inorg. Chem.* **2017**, *56* (5), 3055−3070.
(32) Loewe, R. S.; Ambroise, A.; Muthukumaran, K.; Padmaja, K.; Lysenko, A. B.; Mathur, G.; Li, Q. L.; Bocian, D. F.; Misra, V.; Lindsey, J. S. Porphyrins bearing mono or tripodal benzylphosphonic acid tethers for attachment to oxide surfaces. *J. Org. Chem.* **2004**, *69* (5), 1453−1460.
(33) Li, Q. L.; Surthi, S.; Mathur, G.; Gowda, S.; Zhao, Q.; Sorenson, T. A.; Tenent, R. C.; Muthukumaran, K.; Lindsey, J. S.; Misra, V. Multiple-bit storage properties of porphyrin monolayers on SiO_2. *Appl. Phys. Lett.* **2004**, *85* (10), 1829−1831.
(34) Kubat, P.; Lang, K.; Anzenbacher, P. Modulation of porphyrin binding to serum albumin by pH. *Biochim. Biophys. Acta, Gen. Subj.* **2004**, *1670* (1), 40−48.
(35) Morisue, M.; Haruta, N.; Kalita, D.; Kobuke, Y. Efficient charge injection from the S-2 photoexcited state of special-pair mimic porphyrin assemblies anchored on a titanium-modified ITO anode. *Chem. - Eur. J.* **2006**, *12* (31), 8123−8135.
(36) Officer, D. L.; Lodato, F.; Jolley, K. W. Zinc-porphyrin phosphonate coordination: Structural control through a zinc phosphoryl-oxygen interaction. *Inorg. Chem.* **2007**, *46* (12), 4781−4783.
(37) Habdas, J.; Boduszek, B. Synthesis peptidyl phosphonates containing 4-(4'-carboxyphenyl)-10,15,20-tritolylporphyrin. *Heteroat. Chem.* **2008**, *19* (1), 107−111.
(38) Atefi, F.; Arnold, D. P. Porphyrins with metal, metalloid or phosphorus atoms directly bonded to the carbon periphery. *J. Porphyrins Phthalocyanines* **2008**, *12* (7), 801−831.
(39) Borbas, K. E.; Kee, H. L.; Holten, D.; Lindsey, J. S. A compact water-soluble porphyrin bearing an iodoacetamido bioconjugatable site. *Org. Biomol. Chem.* **2008**, *6* (1), 187−194.
(40) Stern, C.; Bessmertnykh-Lemeune, A.; Gorbunova, Y. G.; Tsivadze, A. Y.; Guilard, R. Effect of the anchoring group in porphyrin sensitizers: Phosphonate versus carboxylate linkages. *Turk. J. Chem.* **2014**, *38*, 980−993.
(41) Urbani, M.; Grätzel, M.; Nazeeruddin, M. K.; Torres, T. *Meso*-substituted porphyrins for dye-sensitized solar cells. *Chem. Rev.* **2014**, *114* (24), 12330−12396.
(42) Liu, X.; Li, H.; Zhang, Y.; Xu, B.; A, S.; Xia, H.; Mu, Y. Enhanced carbon dioxide uptake by metalloporphyrin-based microporous covalent triazine framework. *Polym. Chem.* **2013**, *4* (8), 2445−2448.
(43) Griffith, M. J.; Sunahara, K.; Wagner, P.; Wagner, K.; Wallace, G. G.; Officer, D. L.; Furube, A.; Katoh, R.; Mori, S.; Mozer, A. J. Porphyrins for dye-sensitised solar cells: New insights into efficiency-determining electron transfer steps. *Chem. Commun.* **2012**, *48* (35), 4145−4162.
(44) Liu, T. W.; Huynh, E.; MacDonald, T. D.; Zheng, G. Porphyrins for imaging, photodynamic therapy, and photothermal therapy. In *Cancer Theranostics*; Academic Press: Oxford, U.K., 2014; Chapter 14, pp 229−254.
(45) Deniaud, D.; Schollorn, B.; Mansuy, D.; Rouxel, J.; Battioni, P.; Bujoli, B. Synthesis and catalytic properties of manganese porphyrins incorporated into phosphonate networks. *Chem. Mater.* **1995**, *7* (5), 995−1000.
(46) Deniaud, D.; Spyroulias, G. A.; Bartoli, J. F.; Battioni, P.; Mansuy, D.; Pinel, C.; Odobel, F.; Bujoli, B. Shape selectivity for alkane hydroxylation with a new class of phosphonate-based heterogenised manganese porphyrins. *New J. Chem.* **1998**, *22* (8), 901−905.
(47) Clearfield, A. Metal phosphonate chemistry. In *Progress in Inorganic Chemistry*; Karlin, K. D., Ed.; John Wiley & Sons, Inc.: Hoboken, NJ, 1998; pp 371−510.
(48) Queffelec, C.; Petit, M.; Janvier, P.; Knight, D. A.; Bujoli, B. Surface modification using phosphonic acids and esters. *Chem. Rev.* **2012**, *112*, 3777−3807.
(49) Guerrero, G.; Alauzun, J. G.; Granier, M.; Laurencin, D.; Mutin, P. H. Phosphonate coupling molecules for the control of surface/interface properties and the synthesis of nanomaterials. *Dalton Trans.* **2013**, *42* (35), 12569−12585.
(50) Wang, X.-S.; Chrzanowski, M.; Yuan, D.; Sweeting, B. S.; Ma, S. Covalent heme framework as a highly active heterogeneous biomimetic oxidation catalyst. *Chem. Mater.* **2014**, *26* (4), 1639−1644.
(51) Zhao, M.; Ou, S.; Wu, C.-D. Porous metal−organic frameworks for heterogeneous biomimetic catalysis. *Acc. Chem. Res.* **2014**, *47* (4), 1199−1207.
(52) Barona-Castaño, C. J.; Carmona-Vargas, C. C.; Brocksom, J. T.; de Oliveira, T. K. Porphyrins as catalysts in scalable organic reactions. *Molecules* **2016**, *21* (3), 310.
(53) Kadish, K. M.; Chen, P.; Enakieva, Y. Y.; Nefedov, S. E.; Gorbunova, Y. G.; Tsivadze, A. Y.; Bessmertnykh-Lemeune, A.; Stern, C.; Guilard, R. Electrochemical and spectroscopic studies of poly(diethoxyphosphoryl)porphyrins. *J. Electroanal. Chem.* **2011**, *656* (1−2), 61−71.
(54) Fang, Y.; Kadish, K. M.; Chen, P.; Gorbunova, Y.; Enakieva, Y.; Tsivadze, A.; Bessmertnykh-Lemeune, A.; Guilard, R. Electrochemical and spectroelectrochemical studies of β-phosphorylated Zn porphyrins. *J. Porphyrins Phthalocyanines* **2013**, *17* (10), 1035−1045.
(55) Uvarova, M. A.; Sinelshchikova, A. A.; Golubnichaya, M. A.; Nefedov, S. E.; Enakieva, Y. Y.; Gorbunova, Y. G.; Tsivadze, A. Y.; Stern, C.; Bessmertnykh-Lemeune, A.; Guilard, R. Supramolecular assembly of organophosphonate diesters using paddle-wheel com-

DOI: 10.1021/acs.inorgchem.9b00268
Inorg. Chem. XXXX, XXX, XXX−XXX

plexes: First examples in porphyrin series. *Cryst. Growth Des.* **2014**, *14*, 5976−5984.
(56) Fang, Y.; Gorbunova, Y. G.; Chen, P.; Jiang, X.; Manowong, M.; Sinelshchikova, A. A.; Enakieva, Y. Y.; Martynov, A. G.; Tsivadze, A. Y.; Bessmertnykh-Lemeune, A.; Stern, C.; Guilard, R.; Kadish, K. M. Electrochemical and spectroelectrochemical studies of diphosphorylated metalloporphyrins. Generation of a phlorin anion product. *Inorg. Chem.* **2015**, *54* (7), 3501−3512.
(57) Mitra, R.; Bauri, A. K.; Bhattacharya, S. Study of non-covalent interaction between a designed monoporphyrin and fullerenes (C60 and C70) in absence and presence of silver nanoparticles. *Spectrochim. Acta, Part A* **2012**, *96*, 485−492.
(58) Enakieva, Y. Y.; Michalak, J.; Abdulaeva, I. A.; Volostnykh, M. V.; Stern, C.; Guilard, R.; Bessmertnykh-Lemeune, A. G.; Gorbunova, Y. G.; Tsivadze, A. Y.; Kadish, K. M. General and scalable approach to A_2B- and A_2BC-type porphyrin phosphonate diesters. *Eur. J. Org. Chem.* **2016**, *2016* (28), 4881−4892.
(59) Ogi, S.; Sugiyasu, K.; Manna, S.; Samitsu, S.; Takeuchi, M. Living supramolecular polymerization realized through a biomimetic approach. *Nat. Chem.* **2014**, *6*, 188−195.
(60) Manka, J. S.; Lawrence, D. S. High yield synthesis of 5,15-diarylporphyrins. *Tetrahedron Lett.* **1989**, *30* (50), 6989−6992.
(61) Kadish, K. M.; Van Caemelbecke, E.; Royal, G. Electrochemistry of metalloporphyrins in nonaqueous media. In *The Porphyrin Handbook*; Kadish, K. M., Smith, K. M., Guilard, R., Eds.; Academic Press: San Diego, CA, 2000; Vol. *8*, pp 1−114.
(62) Sinelshchikova, A. A.; Nefedov, S. E.; Enakieva, Y. Y.; Gorbunova, Y. G.; Tsivadze, A. Y.; Kadish, K. M.; Chen, P.; Bessmertnykh-Lemeune, A.; Stern, C.; Guilard, R. Unusual formation of a stable 2D copper porphyrin network. *Inorg. Chem.* **2013**, *52* (2), 999−1008.
(63) Zubatyuk, R. I.; Sinelshchikova, A. A.; Enakieva, Y. Y.; Gorbunova, Y. G.; Tsivadze, A. Y.; Nefedov, S. E.; Bessmertnykh-Lemeune, A.; Guilard, R.; Shishkin, O. V. Insights into the crystal packing of phosphorylporphyrins based on the topology of their intermolecular interaction energies. *CrystEngComm* **2014**, *16*, 10428−10438.
(64) Le Mest, Y.; L'Her, M.; Hendricks, N. H.; Kim, K.; Collman, J. P. Electrochemical and spectroscopic properties of dimeric cofacial porphyrins with nonelectroactive metal centers. Delocalization processes in the porphyrin.pi.-cation-radical systems. *Inorg. Chem.* **1992**, *31* (5), 835−847.
(65) Kemp, R. H.; Thomas, W. A.; Gordon, M.; Griffin, C. E. The proton magnetic resonance spectra of some triheteroarylphosphine oxides and heteroarylphosphonates. *J. Chem. Soc. B* **1969**, 527−530.
(66) Pan, L.; Kelly, S.; Huang, X.; Li, J. Unique 2D metalloporphyrin networks constructed from iron(ii) and *meso*-tetra(4-pyridyl)-porphyrin. *Chem. Commun.* **2002**, No. 20, 2334−2335.
(67) Tanaka, A.; Ryuno, A.; Okada, S.; Satake, A.; Kobuke, Y. Dynamic equilibrium of self-assembled cyclic trimer and tetramer of 1-methyl-5-imidazolylcobalt(III)porphyrin. *Isr. J. Chem.* **2005**, *45* (3), 281−291.
(68) Shachter, A. M.; Fleischer, E. B.; Haltiwanger, R. C. Characterization of a 5-pyridyl-10,15,20-triphenylporphyrinatozinc-(II) polymer. *J. Chem. Soc., Chem. Commun.* **1988**, No. 14, 960−961.
(69) Fleischer, E. B.; Shachter, A. M. Coordination oligomers and a coordination polymer of zinc tetraarylporphyrins. *Inorg. Chem.* **1991**, *30* (19), 3763−3769.
(70) Ercolani, G.; Ioele, M.; Monti, D. Physical basis of self-assembly. Part 2. A theoretical and experimental study of the self-assembly of a zinc *meso*-pyridyl porphyrin. *New J. Chem.* **2001**, *25* (6), 783−789.

DOI: 10.1021/acs.inorgchem.9b00268
Inorg. Chem. XXXX, XXX, XXX−XXX